New Quinazolone-Sulfonate Conjugates with Acetohydrazide Linker as Potential Antimicrobial Agents: Design, Synthesis and Molecular Docking Simulations

Asmaa F. Kassem[a,b], Sherif S. Ragab[c], Mohamed A. Omar[b], Najla A. Altwaijry[d], Mohamed Abdelraof[e], Ahmed Temirak[b], Asmaa Saleh[d], Aladdin M. Srour[f,*]

[a]Department of Chemistry, College of Science and Humanities in Al-Kharj, Prince Sattam Bin Abdulaziz University, Al-Kharj, 11942, Saudi Arabia

[b]Chemistry of Natural and Microbial Products Department, Pharmaceutical and Drug Industries Research Institute, National Research Centre, Dokki, Giza, 12622, Egypt

[c]Photochemistry Department, Chemical Industries Research Institute, National Research Centre (NRC), 33 El-Behouth St., Dokki, Giza, P.O. 12622, Egypt

[d]Department of Pharmaceutical Sciences, College of Pharmacy, Princess Nourah bint Abdulrahman University, P.O. Box 84428, Riyadh 11671, Saudi Arabia

[e]Microbial Chemistry Department, National Research Centre, Biotechnology Research Institute, Giza, Egypt.

[f]Department of Therapeutic Chemistry, Pharmaceutical and Drug Industries Research Institute, National Research Centre, Dokki, Giza, 12622, Egypt

Corresponding author
Email address: aladdinsrour@gmail.com

Supporting information

1. Materials and methods:

All reagents and solvents used in chemical syntheses and biological assays were obtained from various commercial suppliers and were used as received without any purification. The names of the chemicals follow the nomenclature of IUPAC. The progress of the chemical reactions was monitored by TLC on pre-coated silica gel 60 F_{245} aluminum plates (Merck) with visualization under UV light, All the solvents and reagents used for the synthesis of the target compounds are freshly opened bottles (Sigma Aldrich) with 99.5% purity (GC). Melting points were recorded on a Stuart SMP30 melting point apparatus with open capillary tubes and are uncorrected. Elemental analysis of the Quinazolone-Sulfonate derivatives was recorded in the Micro-analytical labs at National Research Centre, Cairo, Egypt. IR spectra (KBr) were recorded on a JASCO 6100 spectrophotometer and NMR spectra were recorded on a JEOL AS 500 (^{1}H: 500 MHz, ^{13}C: 125 MHz) and spectrometer. The purity of the final compounds was determined by LC-MS using the area percentage method on the UV trace recorded at a wavelength of 254 nm and found to be >95%.

The HPLC runs

The experiments utilized a Macherey-Nagel Nucleodur C18 Gravity EC50/2 column (3 µm particle size) set to a temperature of 25 °C. A 1 mg/mL sample solution prepared in acetonitrile was injected (1 µL), and the analysis was conducted at a flow rate of 0.3 mL/min. The initial mobile phase, consisting of 90% water and 10% acetonitrile with 2 mM ammonium acetate, was held for 1 minute before initiating a gradient that reached 100% acetonitrile within 9 minutes. The column was subsequently rinsed with acetonitrile for an additional 5 minutes.

Investigation of the antimicrobial susceptibility of the synthesized compounds

To evaluate the efficiency of the prepared molecules to serve as bactericidal and fungicidal, some clinical microbial pathogenes were tested against the prepared molecules. Bacterial pathogens like *Bacillus subtilis*, *Staphylococcus aureus* (Gram-positive bacteria), *Pseudomonas, aeruginosa*, *Klebsiella pneumonia*, *Sallmonella typhemerium* (Gram-negative bacteria), and *Candida albicans* (unicellular fungal) was kindly donated by Microbiology and Immunology Dep., Faculty of Medicine (Boys), Al-Azhar University. Before the antimicrobial examination, each pathogen was preactivated using a Nutrient broth medium (Codalab, Spain) at 37^{o}C for 24 h. for bacterial pathogen or Potato Dextrose broth (Biolife, Italy) at 28^{o}C for 48 h. for *Candida albicans* refreshed. Accurately, justification of inoculum size for each pathogen was carried out using Colony Forming Unite (CFU) to be constant throughout all performed tests. In this way, the agar well diffusion method was selected for the screening of the synthesized molecules at a constant concentration (20 μg/mL) compared to the standard antibacterial (Cephradine, Ciprofloxacin), and antifungal (Flucanazole, Amphotrecine B) agents. After the incubation period, the obtained results of the selected molecules and standard antimicrobial agents were measured based on the inhibition zone diameter (mm) around each pathogen [1-4]. Subsequently, the potent molecules demonstrated significant antimicrobial activity and were subjected to an assessment of the Minimum Inhibition Concentration (MIC) value. In this regard, each targeted molecule was diluted to obtain a desired concentration of 6.25-400 µg/ml, and the broth microdilution method according to CLSI Protocol. In brief, a defined weight for each selected molecule was dissolved in Dimethyl sulphoxide (DMSO) and used as a stock solution [5]. The determination of the MIC value for each targeted compound was known as the lowest concentration of

each sample that yielded a minimum number of colony-forming units (CFU) compared to the untreated samples [6].

Effect of the targeted synthesized compounds on the bacterial lipid peroxidation (LPO)

Oxidative stress on the bacterial cells was usually indicated by the oxidation of the fatty acid contents in the bacterial cell membrane. The lipid peroxidation marker is an important tool that demonstrated the tested molecules' potential to cause a disruption effect for the lipid content in the bacterial cell membrane. Since the bacterial cell membrane has a considerable content of the fatty acid it changes in amount according to the bacterial cell type, Gram-positive or Gram-negative. Therefore, the treated bacterial cells using the most potent molecules were subjected to investigate the lipid peroxidation process. The lipid peroxidation colorimetric assay kit was used for this purpose, the indication of the fatty acid peroxidation byproduct, Malondialdehyde (MDA) was performed by a specific reagent thiobarbituric acid (TBA) to yield a pink color complex, MDA-TBA [7]. Accordingly, the MIC of each efficient molecule was used to measure the oxidation of the lipid contents in the bacterial cell membrane under standard laser conditions. To assess the LP, 1 mL of each treated bacterial pathogen was vigorously combined with 300 μl MDA lysis buffer at 4^{o}C, and 3 μl of Butylated hydroxytoluene BHT was subsequently added to prevent the pigment interference that resulted from the decomposition of lipophilic peroxides. Each sample was centrifuged at 8000 rpm for 10 minutes, and the insoluble substances were removed. Taking 200 μl of the clear filtrate and mixed with 600 μl of the TBA solution and incubated at 95^{o}C for 60 min. After cooling samples at room temperature, the resulting pink color was read at 532 nm using a Spectrophotometer (Agilent Cary 100, Germany). Treatment of both bacterial pathogens using 5 % Hydrogen peroxide for 20 min. as a positive control was also included. The indicated increase in the lipid peroxidation efficiency was calculated from the following equation. Lipid peroxidation efficiency (%) = [(NC- NS)/NC] X 100. Where NC is the absorbance of lipid peroxidation in the untreated bacterial cells and NS is the absorbance of lipid peroxidation in the treated bacterial cells.

Biofilm inhibition activity of the synthesized molecules:

The compounds being inhibit the biofilm formation was also determined by the crystal violet method [8]. Inoculation of 10 μL of each bacterial pathogen in the 170 μL Mueller Hinton broth using a 96-well culture plate, 10 μL of the targeted molecule was transferred finally to each well in comparison to the control sample (without tested molecule). After cultivation of the plate at 37^{o}C for 24h, the content of the wells was discarded and then washed with 200 μL of phosphate buffer saline (PBS) pH 7.2 to remove any bacterial derbies and drying for 1h. in the sterilized laminar flow. Subsequently, 200 μL/per well of crystal violet (0.1%, w/v) was added for 1hr and the excessive stain was eliminated and the plates were drying.

Confocal laser scanning microscope

The effect of the most potent compounds against microbial pathogens was analyzed by confocal laser scanning microscopy (Leica Microsystems DMi8, GmbH, Wetzlar, Germany). In this way, staining with Acridine orange and propidium iodide was carried out to differentiate the cells as a function of compromised membranes. Confocal illumination was provided with a X63 magnification objective and numerical aperture of 1.40–0.60 and by Argon laser (488 nm laser excitation) with a long pass 520–565 nm filter (for green emission) and long pass 630–685 nm filter (for red emission). Image analysis was performed using FRET and FRAP software (Leica Microsystems GmbH, Wetzlar, Germany) [9,10].

Molecular Docking

A molecular docking study was carried out to evaluate the potential inhibitory effects of a series of new quinazolinone derivatives (**5a-r**) against the DNA gyrase enzyme (PDB code: 6F86). These synthesized compounds' binding interactions and affinities towards the DNA gyrase enzyme were analyzed. The study commenced by retrieving the X-ray structure of the DNA gyrase enzyme from the Protein Data Bank (https://www.rcsb.org) using the specified PDB code (6F86). The receptor preparation was performed using Biovia Discovery Studio, which involved eliminating unnecessary chains and water molecules from the enzyme structure, adding polar hydrogens, and correcting partial charges to create suitable receptor models for docking simulations. The docking studies were conducted using the Autodock 4.2 software package. Initially, the docking protocol was validated by redocking the co-crystallized native ligand into the active site of the DNA gyrase enzyme. The

procedure involved preparing coordinate files for both the docking molecules and the target enzyme. An affinity grid was then calculated for the target molecule, with the grid box size set to 50x50x50 based on the position of the co-crystallized ligand and a grid point spacing of 0.375Å. The search for optimal conformations was performed using the Lamarckian Genetic Algorithm (LGA), running 10 sets of the Genetic Algorithm (GA), each simulating up to 27,000 generations. The mutation rate was set to 0.02, and the crossover rate to 0.8. Multiple runs of AutoDock 4.2 generated several docked conformations, with the best solutions identified by evaluating the predicted energy and the consistency of results.

Table S1. Antimicrobial activity of the targeted molecules using agar-well diffusion

Sample ID.	Inhibition Zone (mm)					
	Candida albicans	*Staphylococcus aureus* MRSA	*Bacillus cereus*	*Salmonella typhimurium*	*Klebsiella pneumonia*	*Pseudomonas aeruginosa*
5a	**4**	**2**	**2**	ND	**3**	ND
5b	3	3	ND	ND	2	ND
5c	ND	2	ND	ND	3	ND
5d	3	ND	ND	ND	3	ND
5e	3	3	ND	ND	ND	3
5f	**4**	**4**	**3**	**2**	**2**	**2**
5g	**4**	**3**	**2**	**3**	**2**	**2**
5h	**4**	3	ND	ND	3	ND
5i	2	2	ND	ND	2	ND

5j	2	ND	ND	2	2	ND
5k	**3**	**2**	**2**	**3**	**2**	**2**
5l	ND	2	ND	ND	3	ND
5m	ND	ND	ND	ND	2	ND
5n	2	ND	3	ND	ND	ND
5o	ND	ND	2	ND	2	2
5p	ND	ND	ND	ND	3	3
5q	ND	ND	ND	ND	2	ND
5r	ND	2	ND	ND	2	ND
Fluconazole[a]	ND	-				
Amphotericin B[a]	4	-				
Ciprofloxacin[b]	-	3	5	4	5	3
Cephradine[b]	-	-	ND	ND	ND	ND
Sulfadiazine	3	2	3	ND	2	ND

[a] Fluconazole and Amphotericin were used as standard antifungal agents at 20 μg/ mL,
[b] Ciprofloxacin and Cephradine were used as standard antibacterial agents at 20 μg/mL,
[c] ND: not determined.

Table S2: Percentage cytotoxicity of compounds **5f**, **5g** and **5k** at 100 μM against (**BJ1**).

Compd. No.	The percentage cytotoxicity at 100 μM*
5f	52.43 ± 3.58
5g	75.60 ± 2.33
5k	68.12 ± 4.48

*Percentage cytotoxicity of the compounds tested at 100 μM on BJ1.

Table S3. The flexible docking results (AutoDock 4.2), regarding the binding free energies (ΔG_b) between the synthesized compounds **5a-r** and the amino acid residues of DNA gyrase enzyme (PDB code: 6F86).

Compound	**ΔG_b[a] (kcal/mol)**	**RMSD[b]**
5a	-9.60	1.43
5b	-8.26	0.95

5c	-8.09	1.45
5d	-7.86	1.24
5e	-8.22	1.29
5f	-10.12	1.37
5g	-9.85	1.36
5h	-9.80	0.62
5i	-7.62	0.69
5j	-8.16	1.33
5k	-10.55	1.47
5l	-7.01	1.12
5m	-8.87	1.03
5n	-7.49	1.24
5o	-7.58	1.19
5p	-9.24	1.01
5q	-7.99	1.23
5r	-9.27	0.99
CWW[b] (native ligand)	-11.72	0.65
Ciprofloxacin	-10.88	0.95

[a] Binding free energy
[b] Root Mean Square Deviation
[c] 4-(4-bromo-1*H*-pyrazol-1-yl)-6-[(ethylcarbamoyl)amino]-*N*-(pyridin-3-yl)pyridine- 3-carboxamide

Pseudomonas aeruginosa	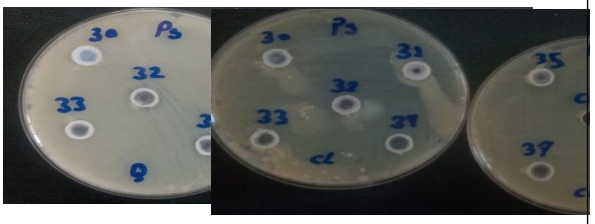

Salmonella typhimurium	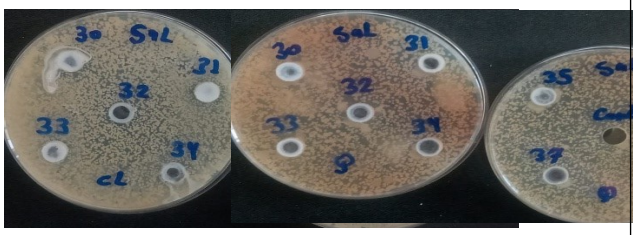
Klebsiella pneumonia	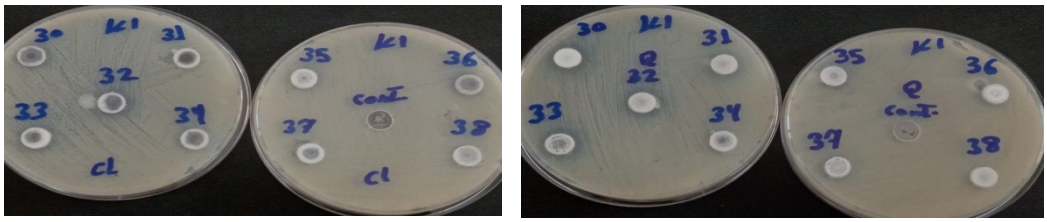
Staphylococcus aureus	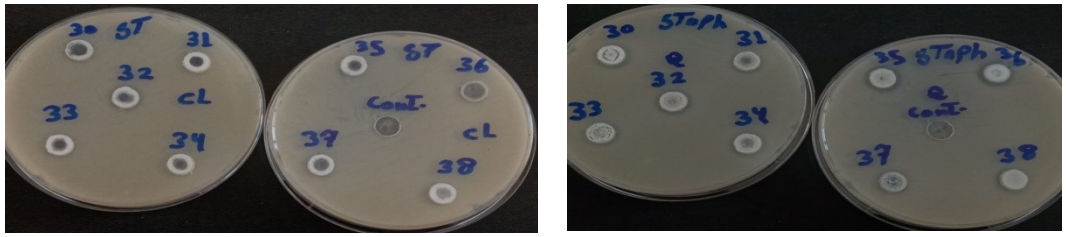
Bacillus subtilis	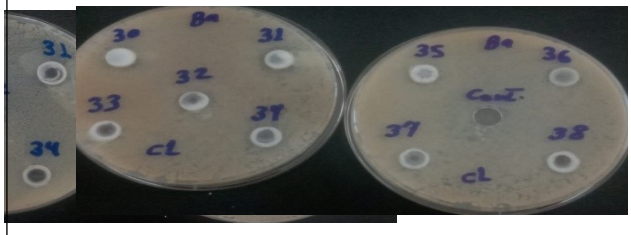

Candida albicans	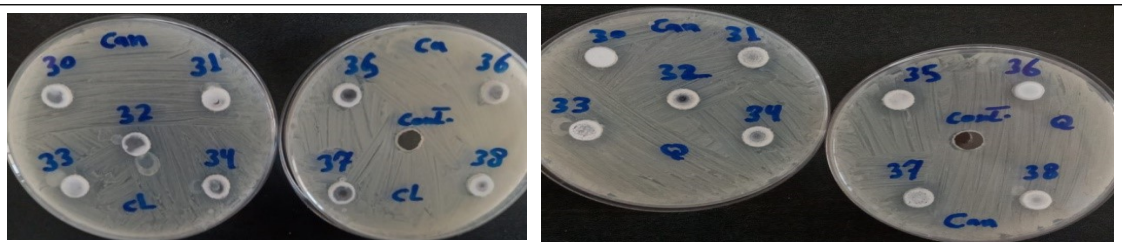

Fig. S1. Antimicrobial activity of the targeted molecules using Agar well diffusion method where: Q30 (**5a**), Q31 (**5b**), Q32 (**5c**), Q33 (**5d**), Q34 (**5e**), Q35 (**5f**), Q36 (**5g**), Q37 (**5h**), Q38 (**5i**), Cl30 (**5j**), Cl31 (**5k**), Cl32 (**5l**), Cl33 (**5m**), Cl34 (**5n**), Cl35 (**5o**), Cl36 (**5p**), Cl37 (**5q**), Cl38 (**5r**). Cont. (Control), Ps (*Pseudomonas aeruginosa*), Sal. (*Salmonella typhimurium*), Kl (*Klebsiella pneumonia*), St (*Staphylococcus aureus*), Ba (B*acillus subtilis*), Can (*Candida albicans*).

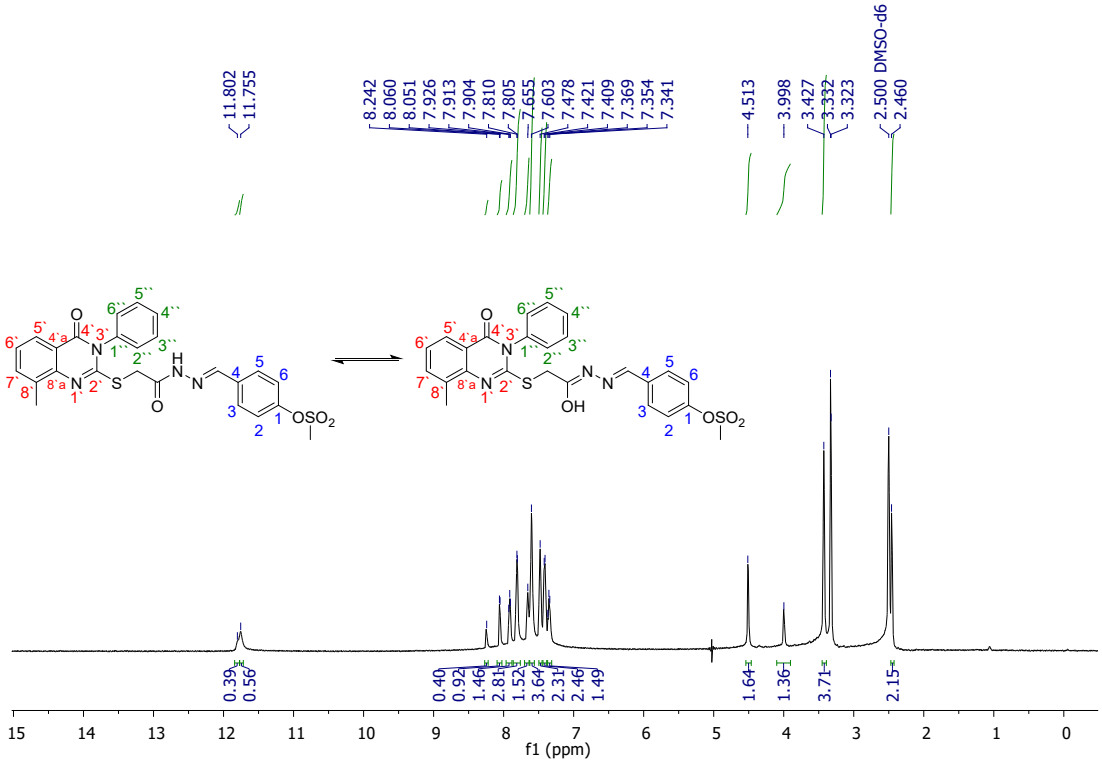

Fig. S2. ^{1}H NMR spectrum of compound **5a**.

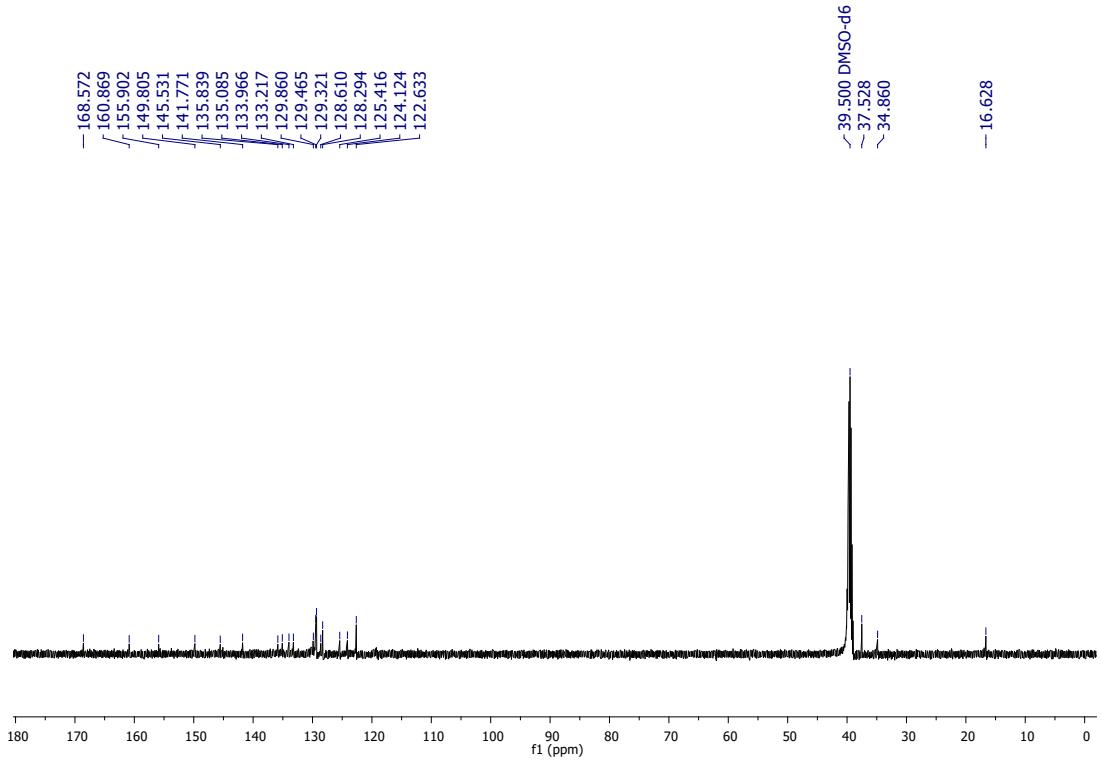

Fig. S3. ^{13}C NMR spectrum of compound **5a**.

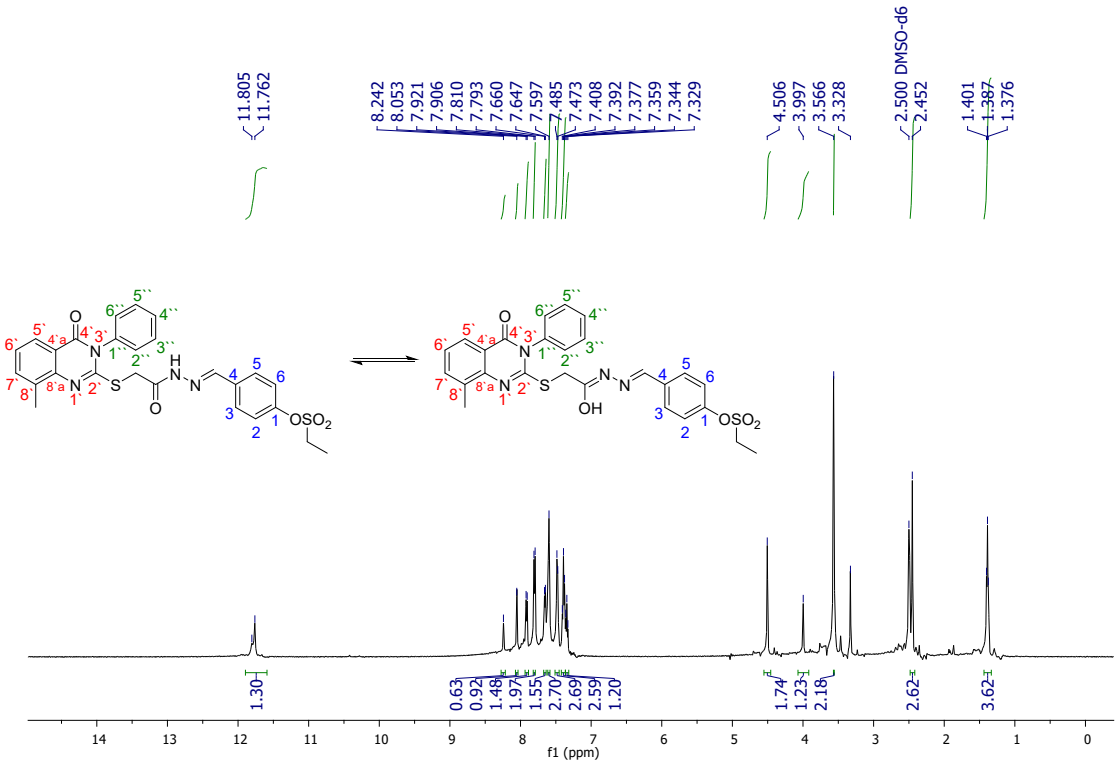

Fig. S4. ^{1}H NMR spectrum of compound **5b**.

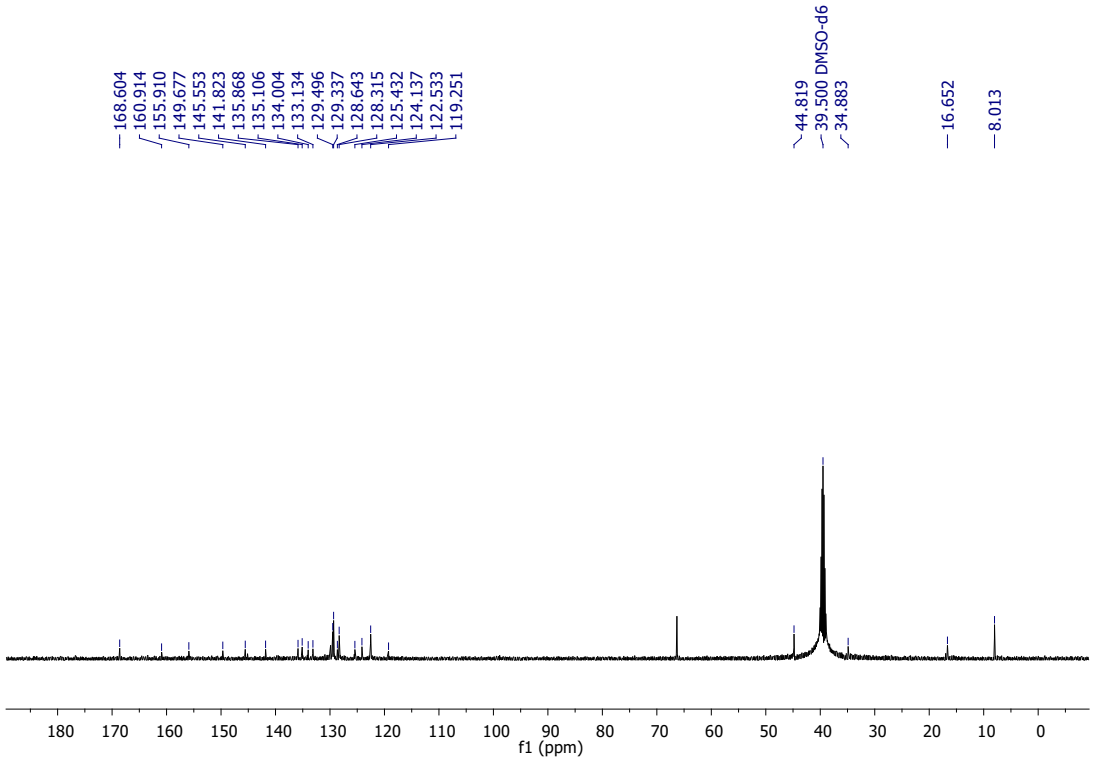

Fig. S5. ^{13}C NMR spectrum of compound **5b**.

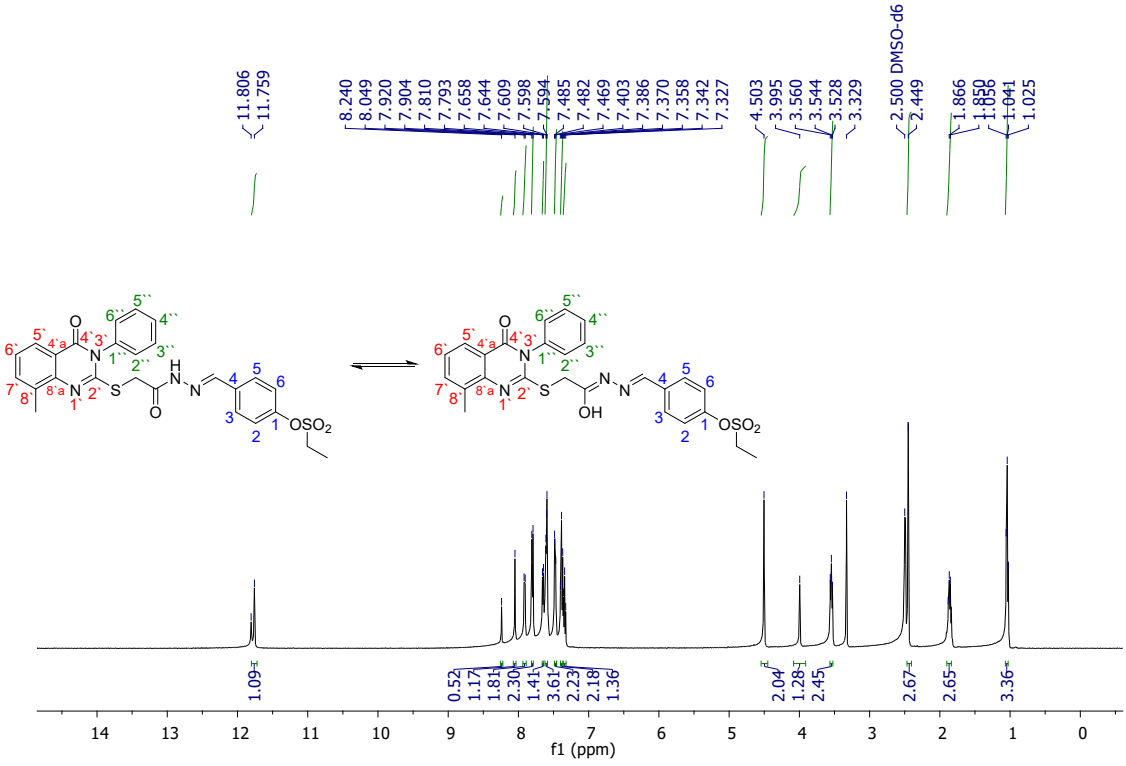

Fig. S6. ^{1}H NMR spectrum of compound **5c**.

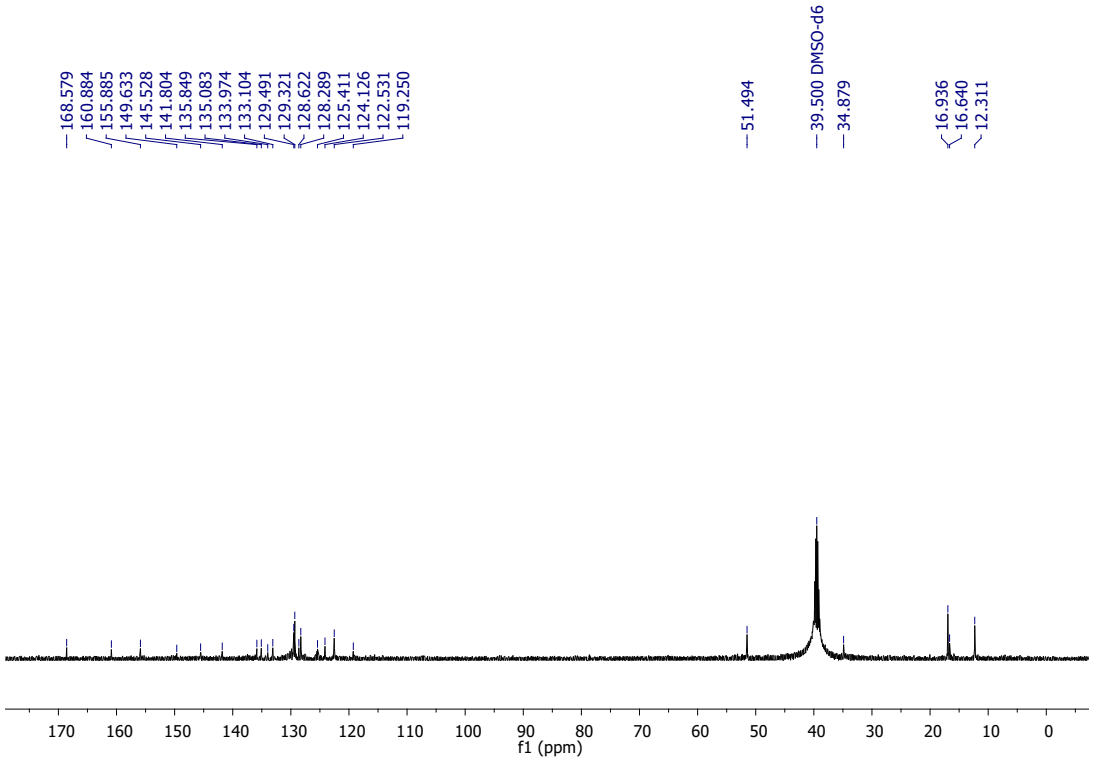

Fig. S7. ^{13}C NMR spectrum of compound **5c**.

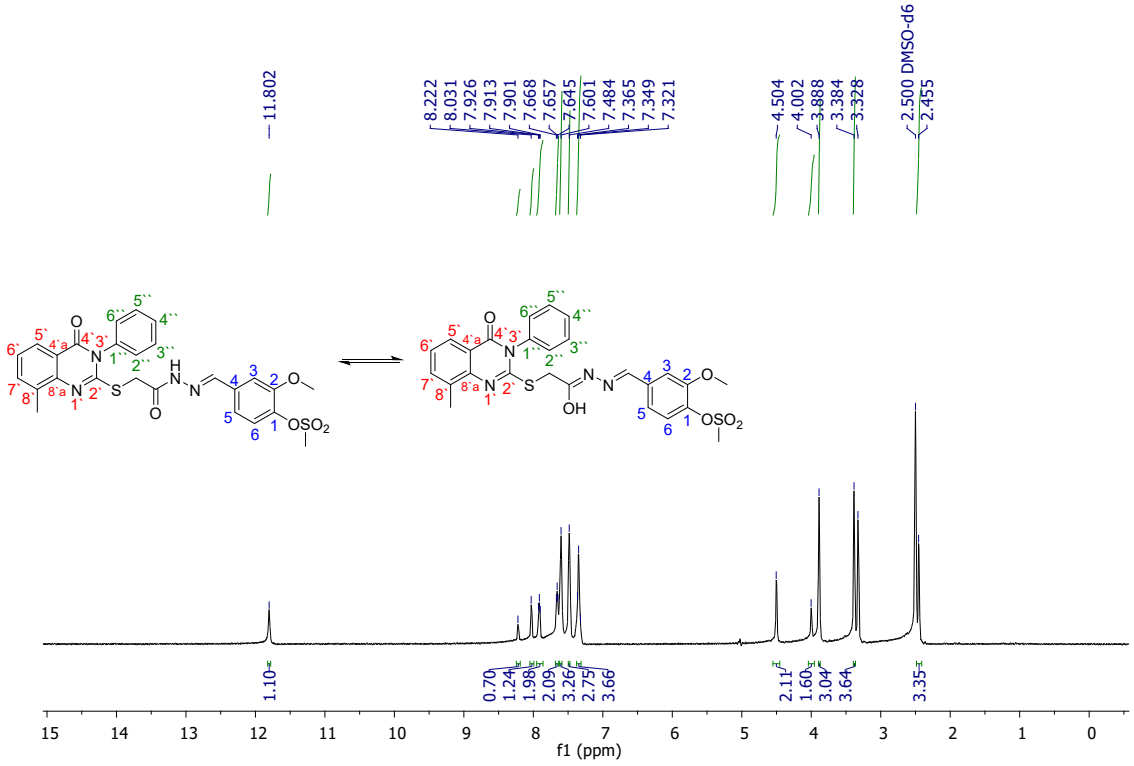

Fig. S8. ^{1}H NMR spectrum of compound **5d**.

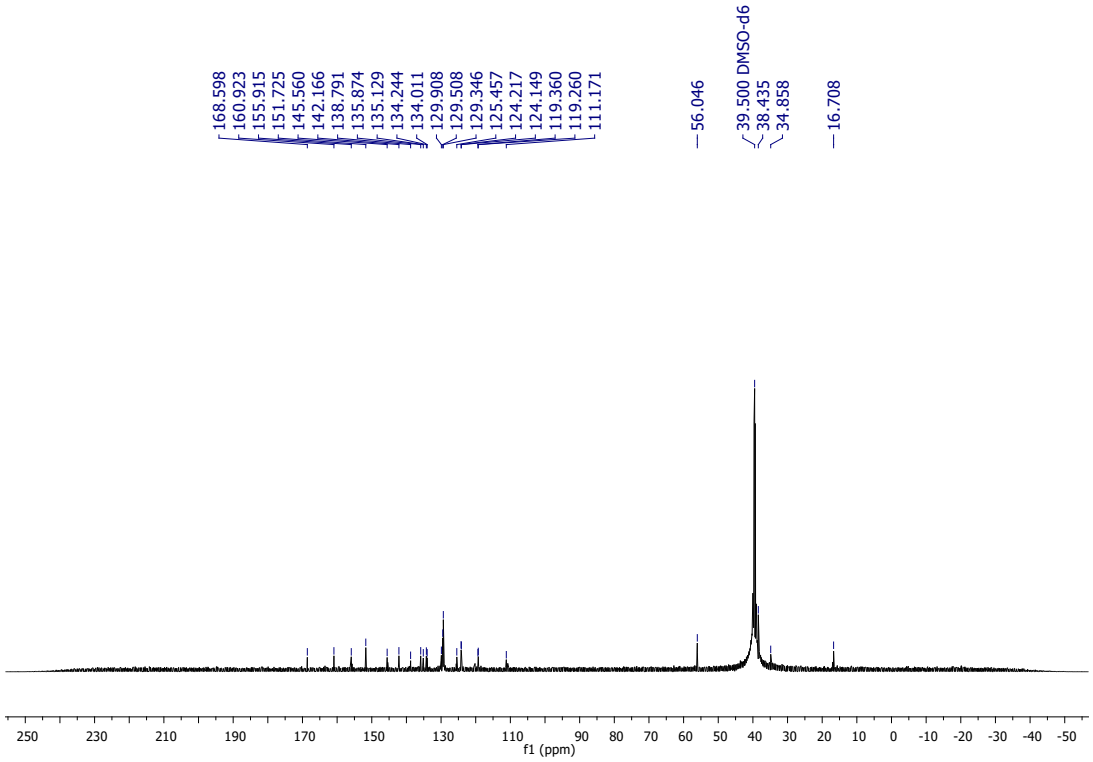

Fig. S9. ^{13}C NMR spectrum of compound **5d**.

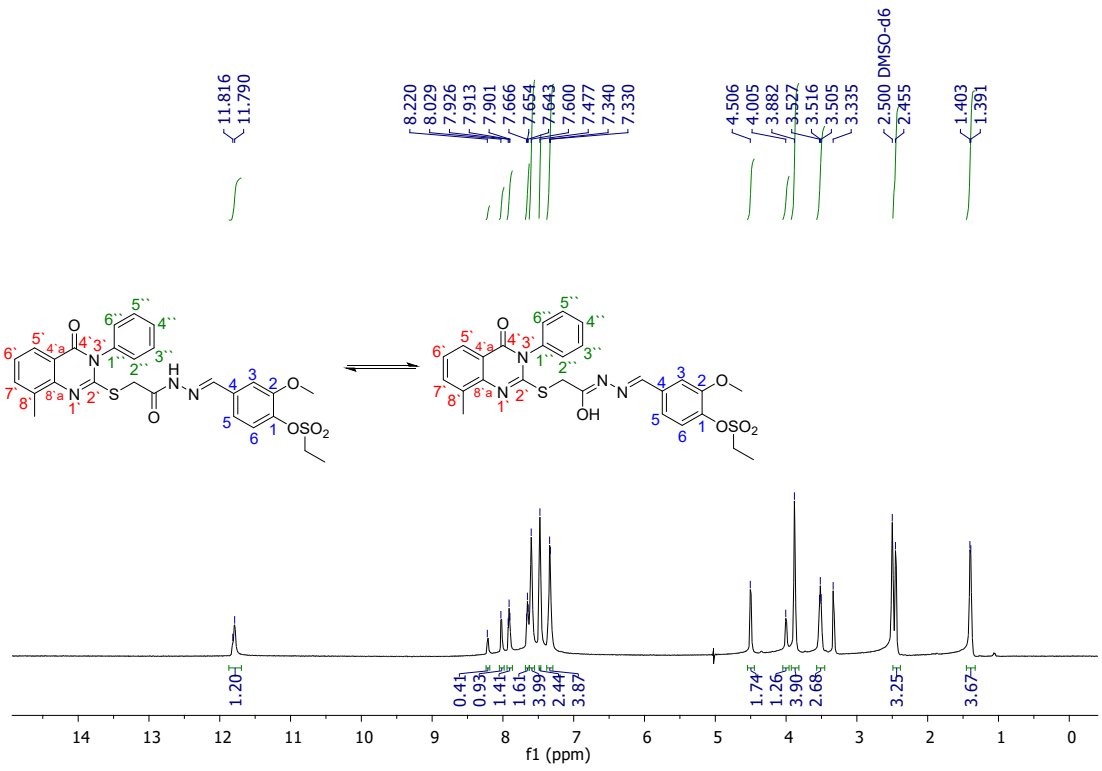

Fig. S10. ^{1}H NMR spectrum of compound **5e**.

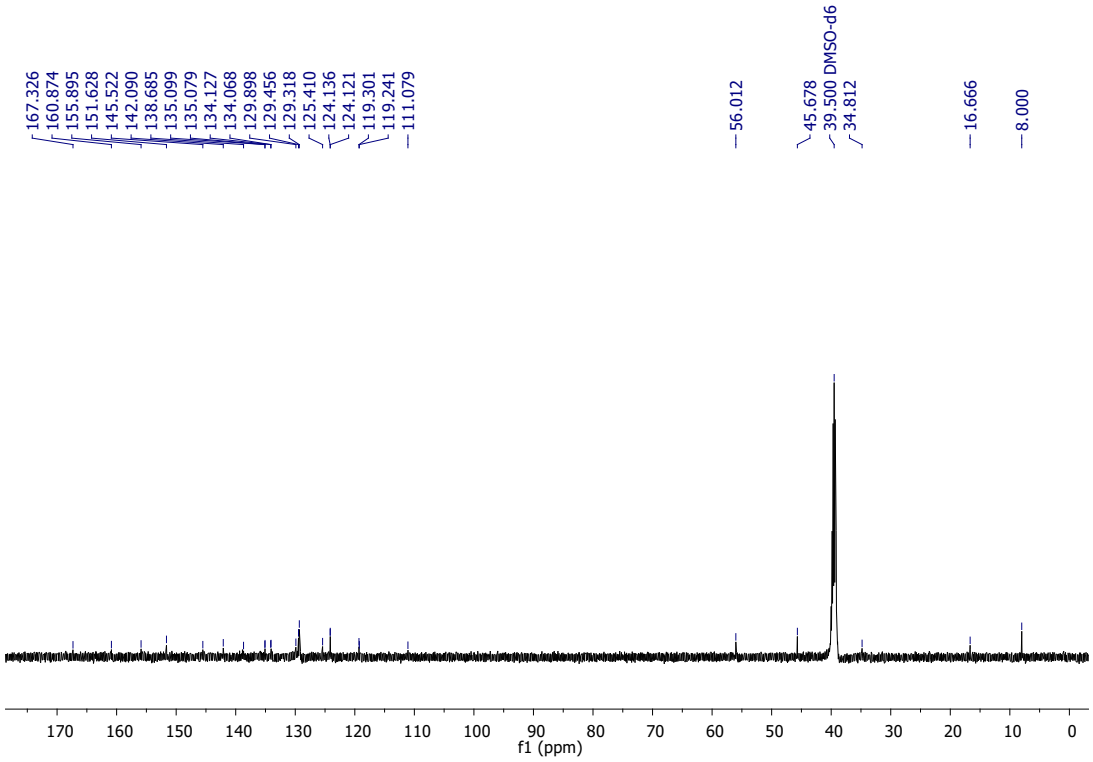

Fig. S11. ^{13}C NMR spectrum of compound **5e**.

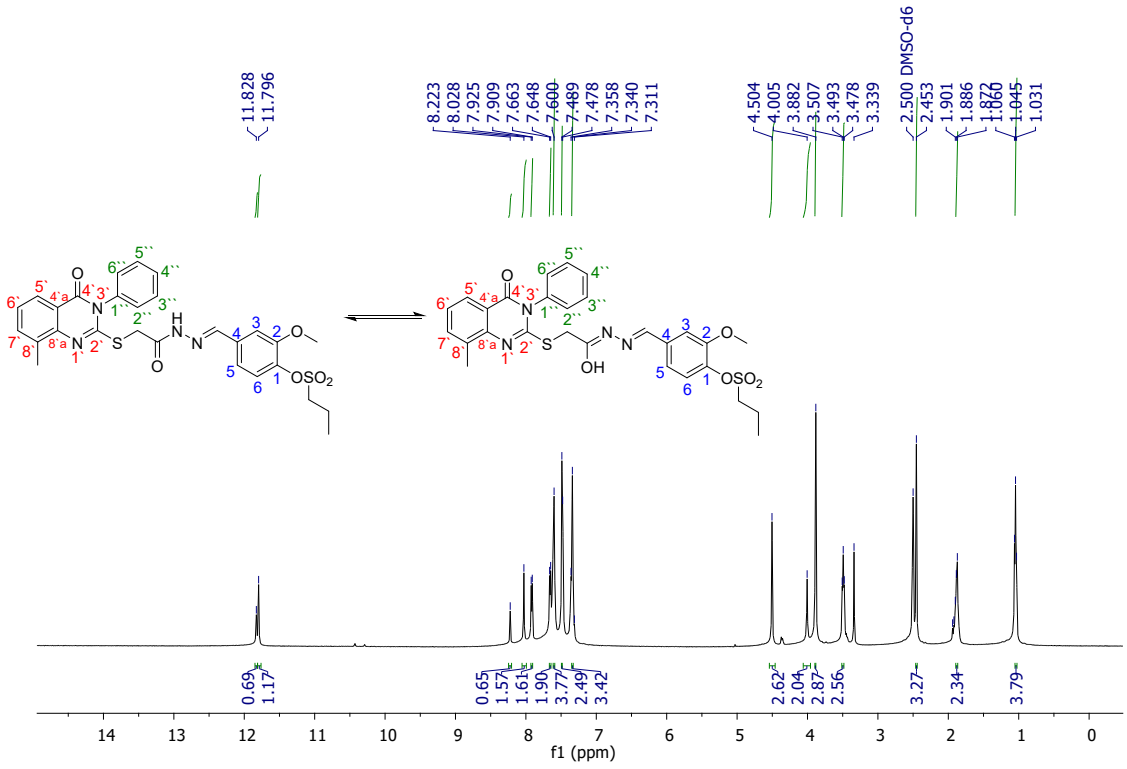

Fig. S12. ^{1}H NMR spectrum of compound **5f**.

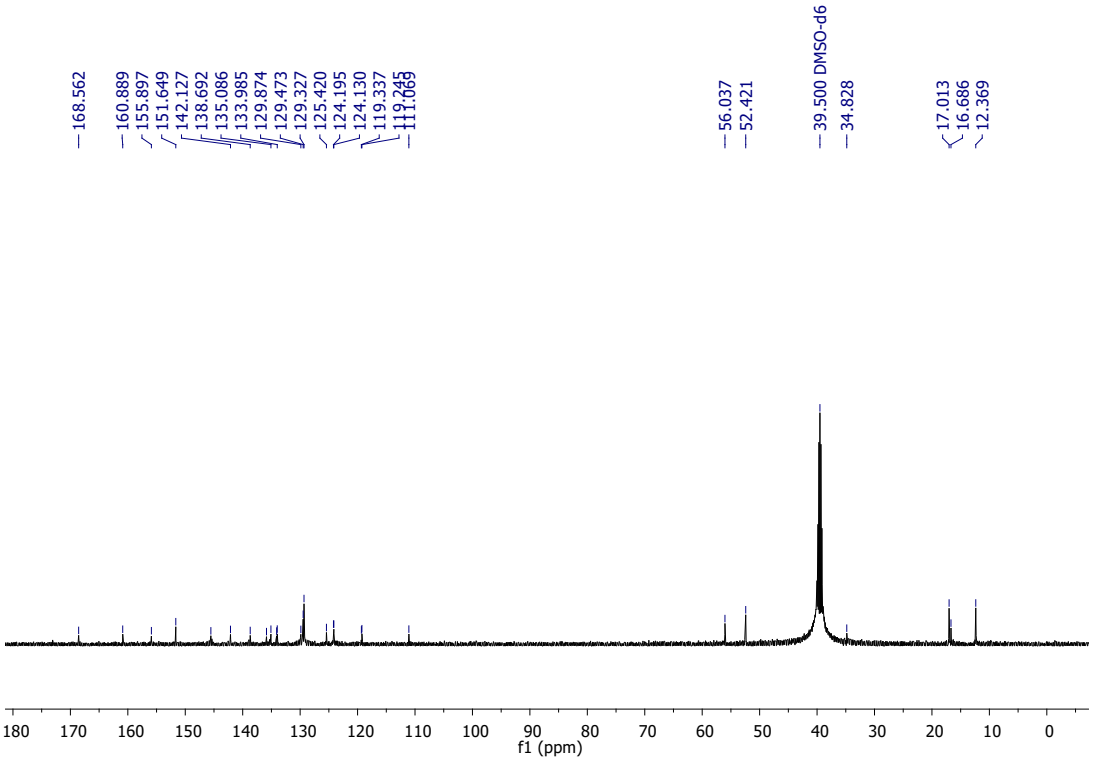

Fig. S13. ^{13}C NMR spectrum of compound **5f**.

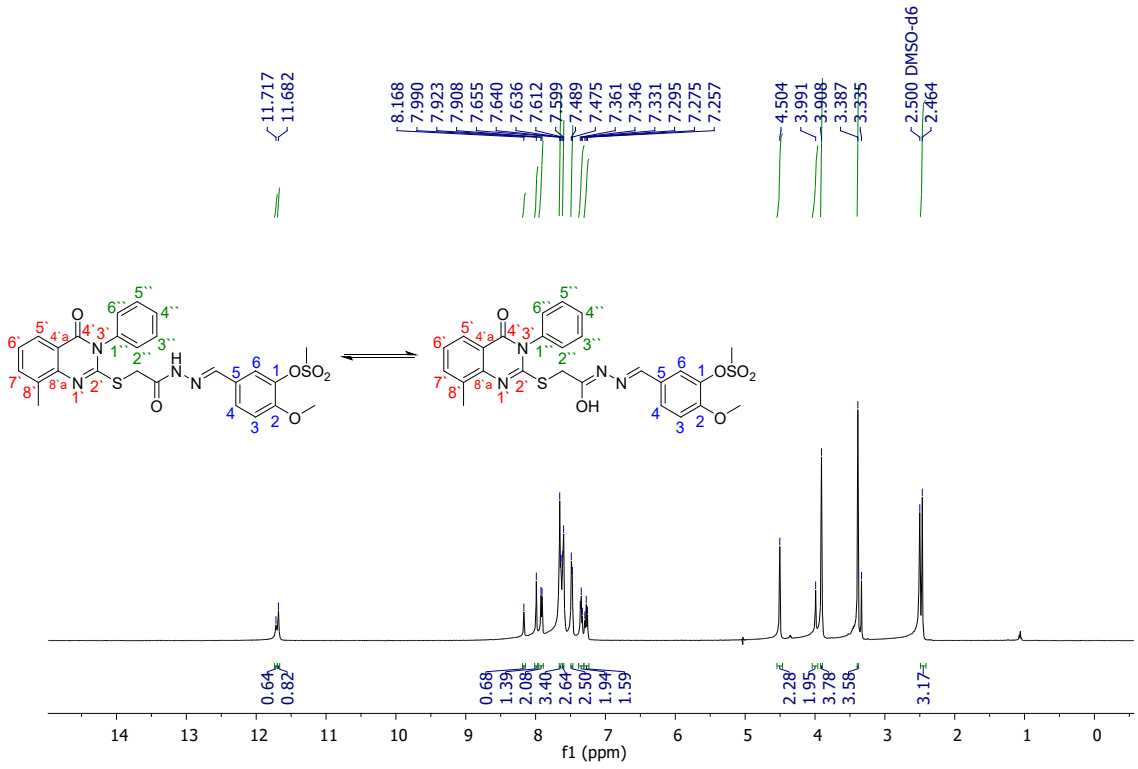

Fig. S14. ^{1}H NMR spectrum of compound **5g**.

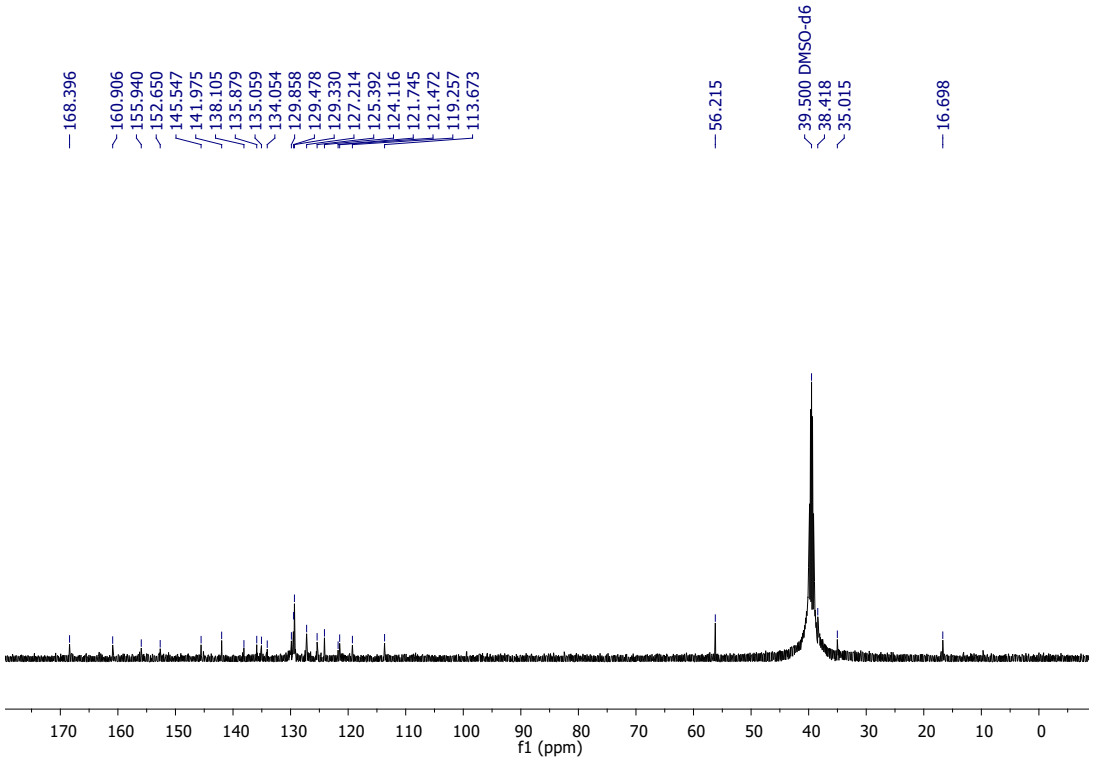

Fig. S15. ^{13}C NMR spectrum of compound **5g**.

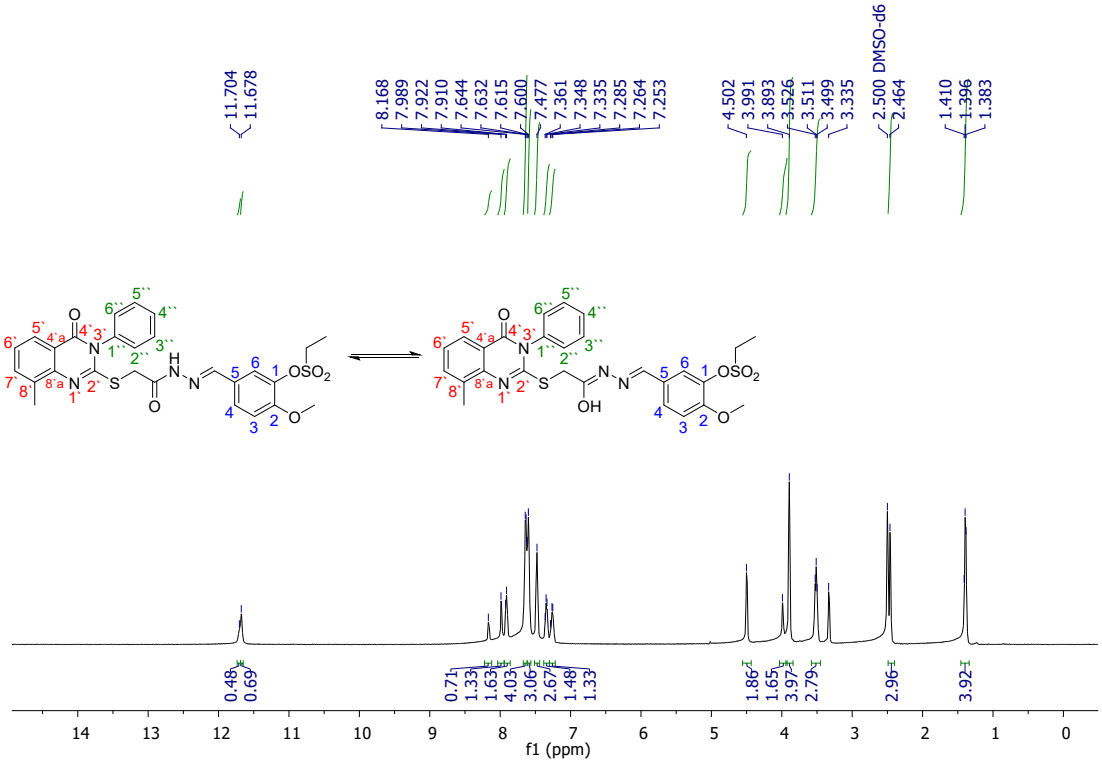

Fig. S16. ^{1}H NMR spectrum of compound **5h**.

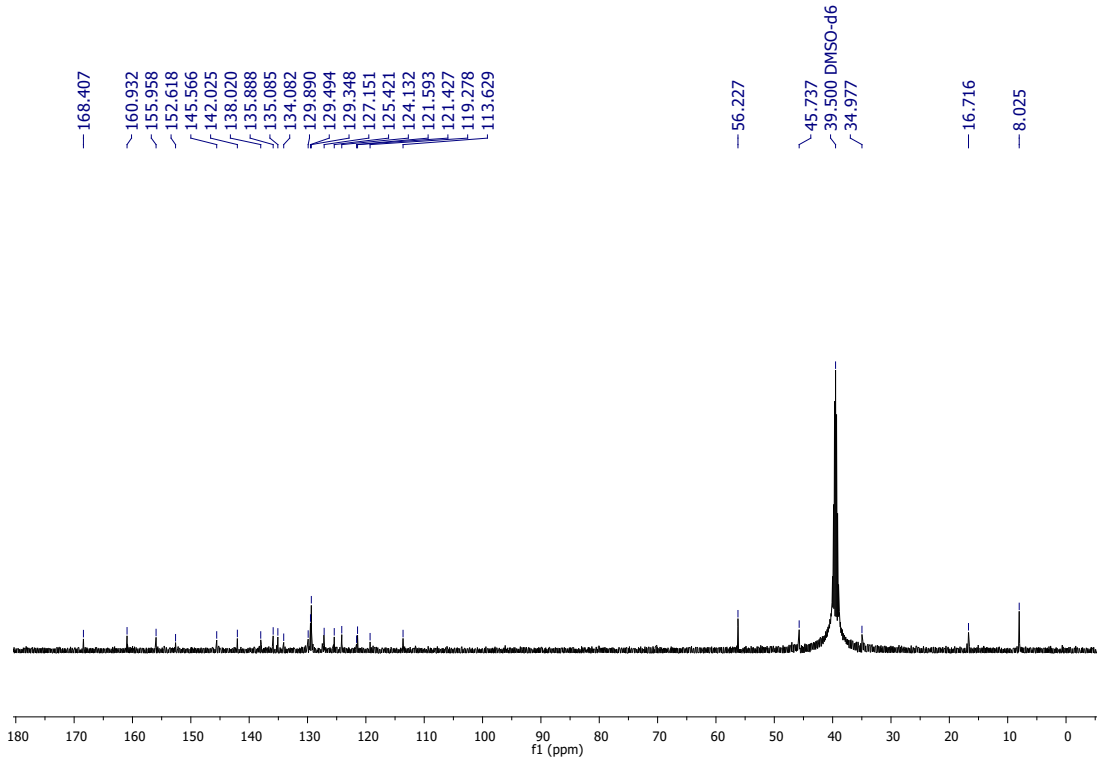

Fig. S17. ^{13}C NMR spectrum of compound **5h**.

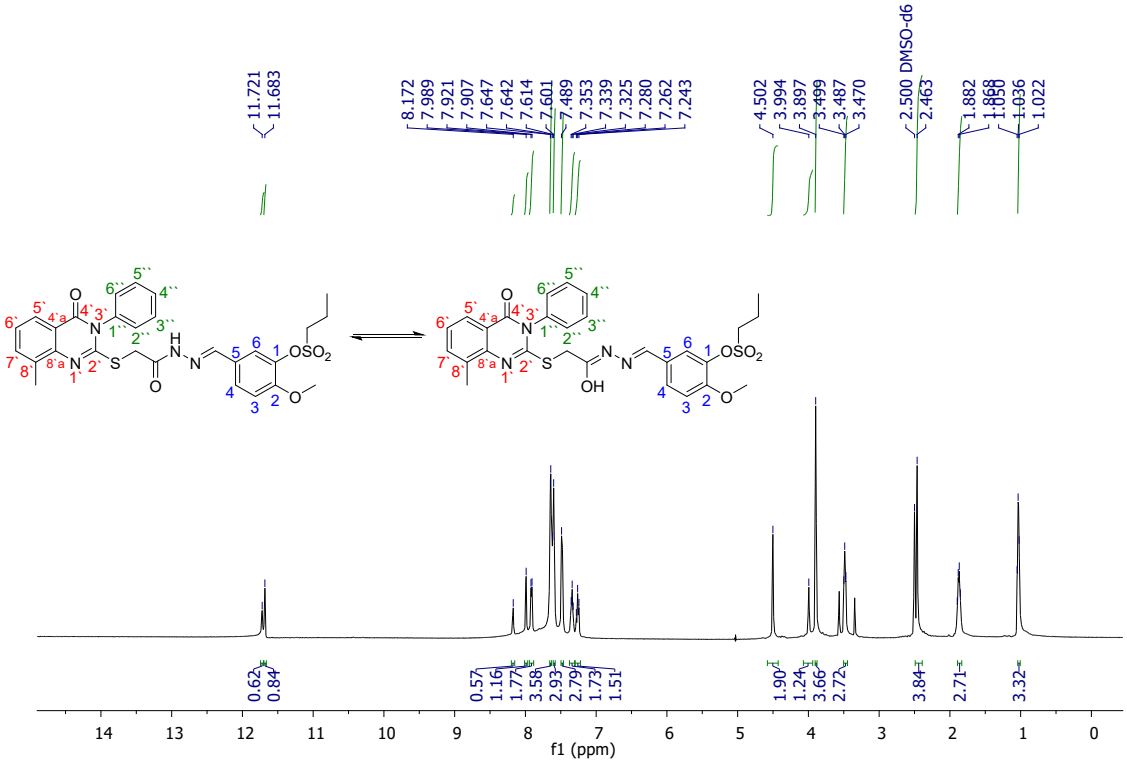

Fig. S18. ^{1}H NMR spectrum of compound **5i**.

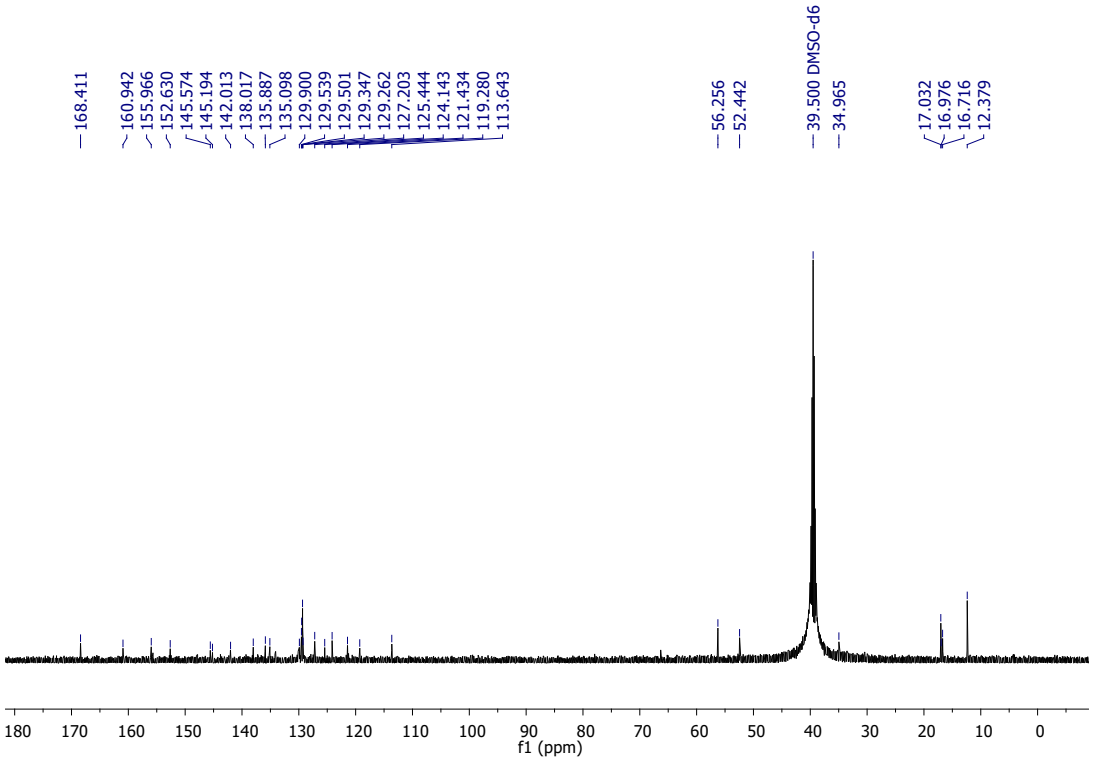

Fig. S19. ^{13}C NMR spectrum of compound **5i**.

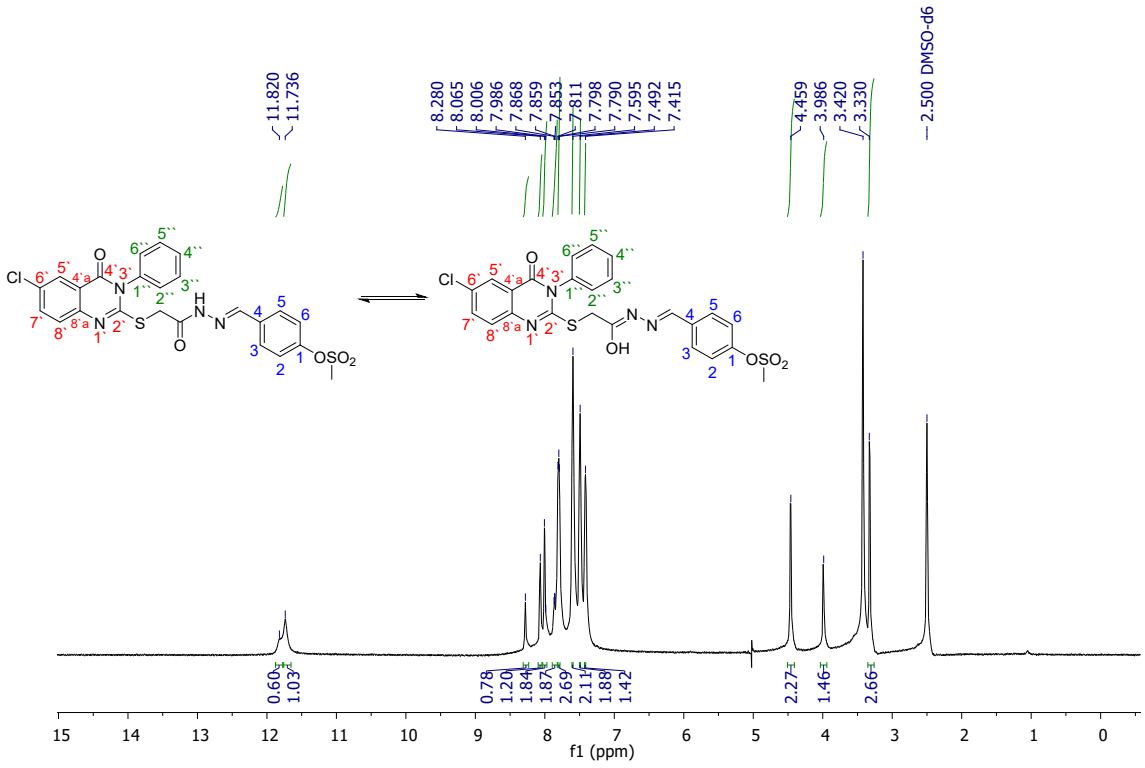

Fig. S20. ^{1}H NMR spectrum of compound **5j**.

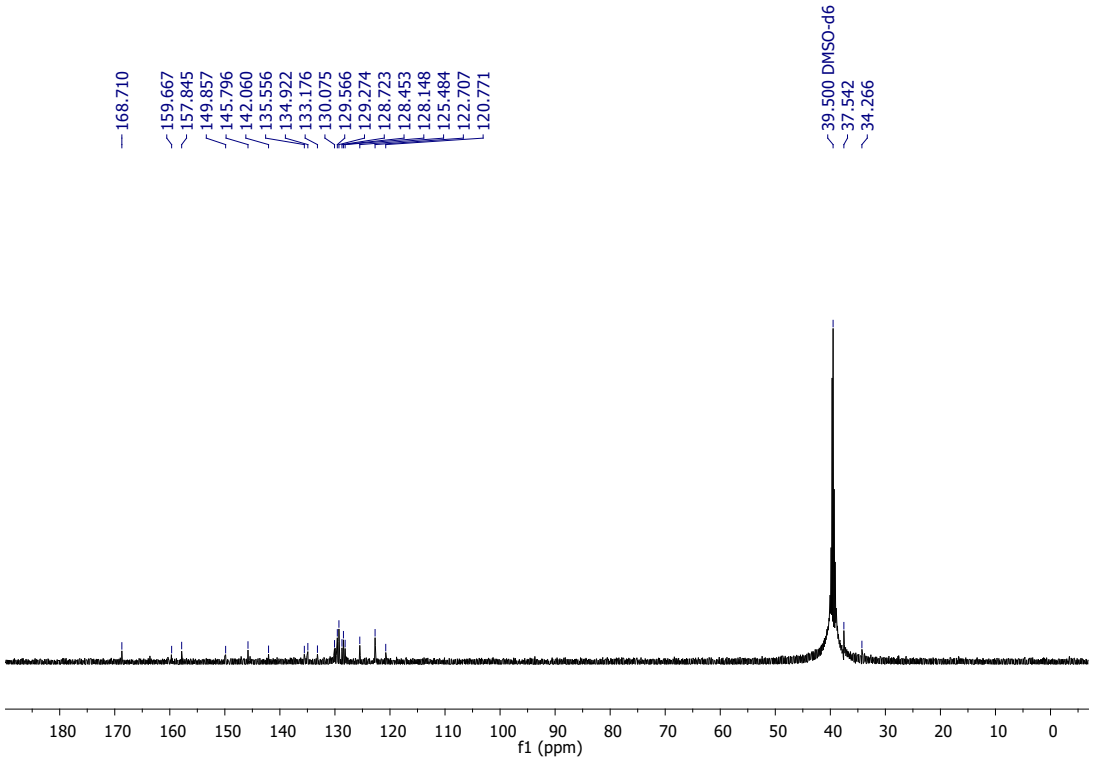

Fig. S21. ^{13}C NMR spectrum of compound **5j**.

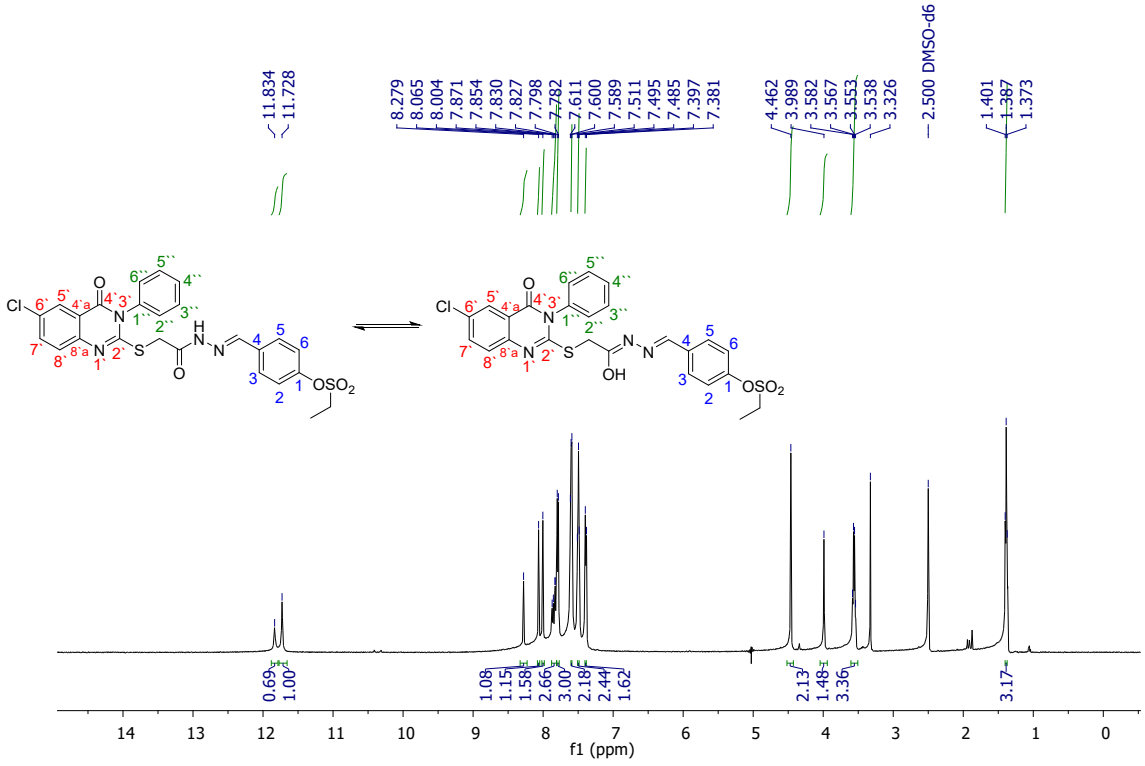

Fig. S22. ^{1}H NMR spectrum of compound **5k**.

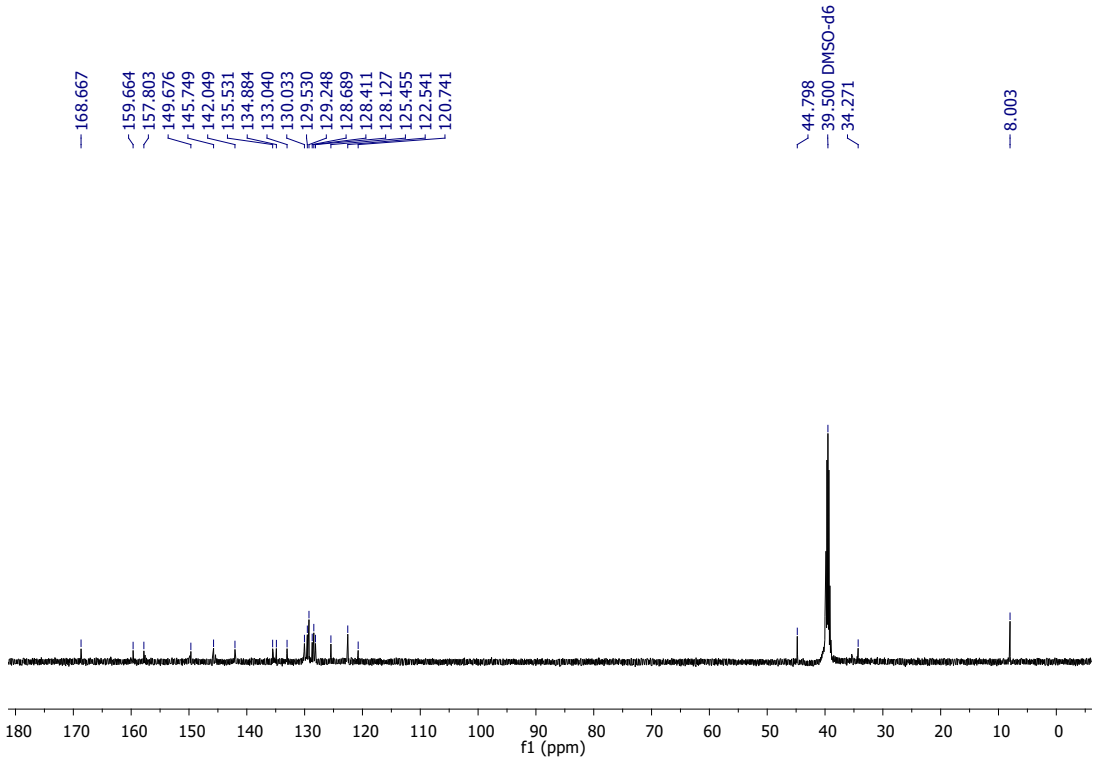

Fig. S23. ^{13}C NMR spectrum of compound **5k**.

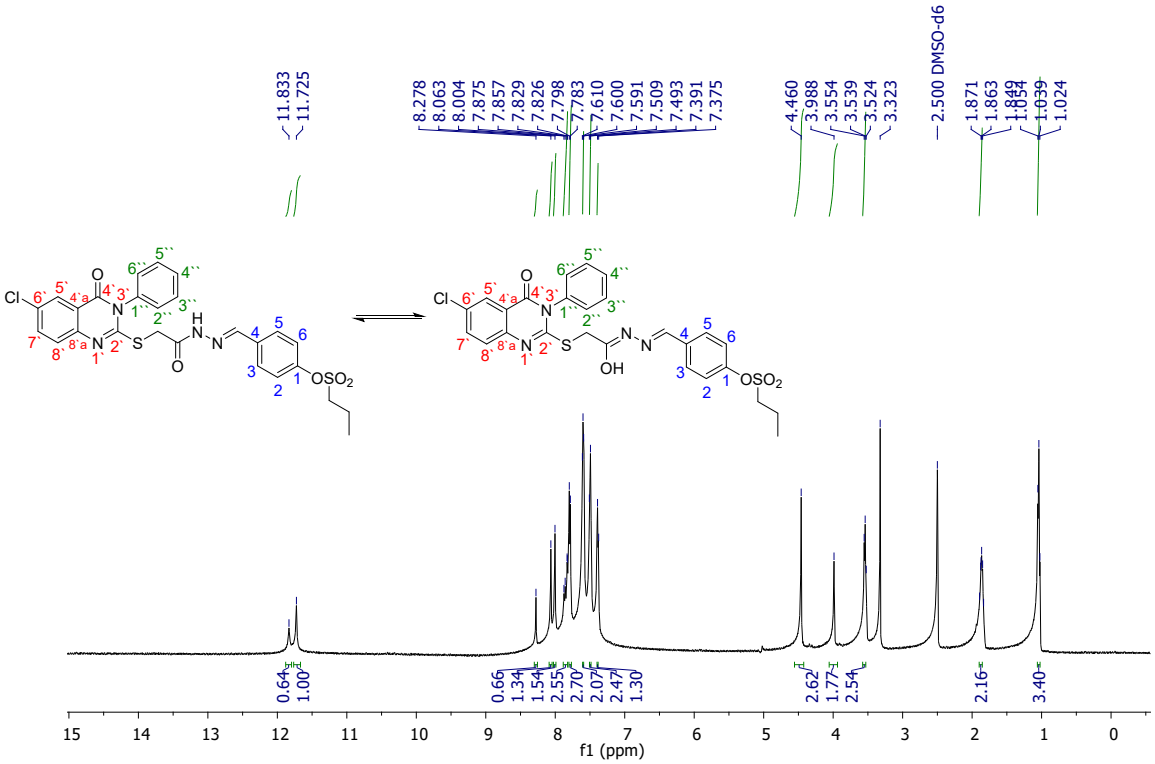

Fig. S24. ^{1}H NMR spectrum of compound **5l**.

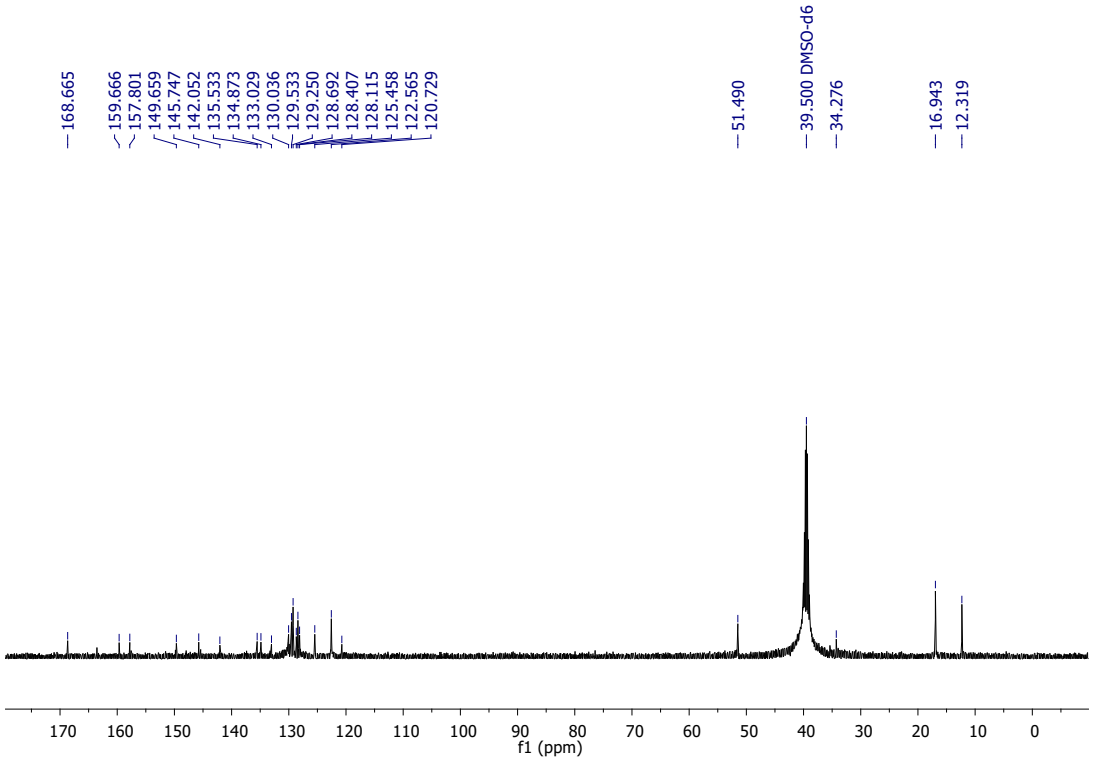

Fig. S25. ^{13}C NMR spectrum of compound **5l**.

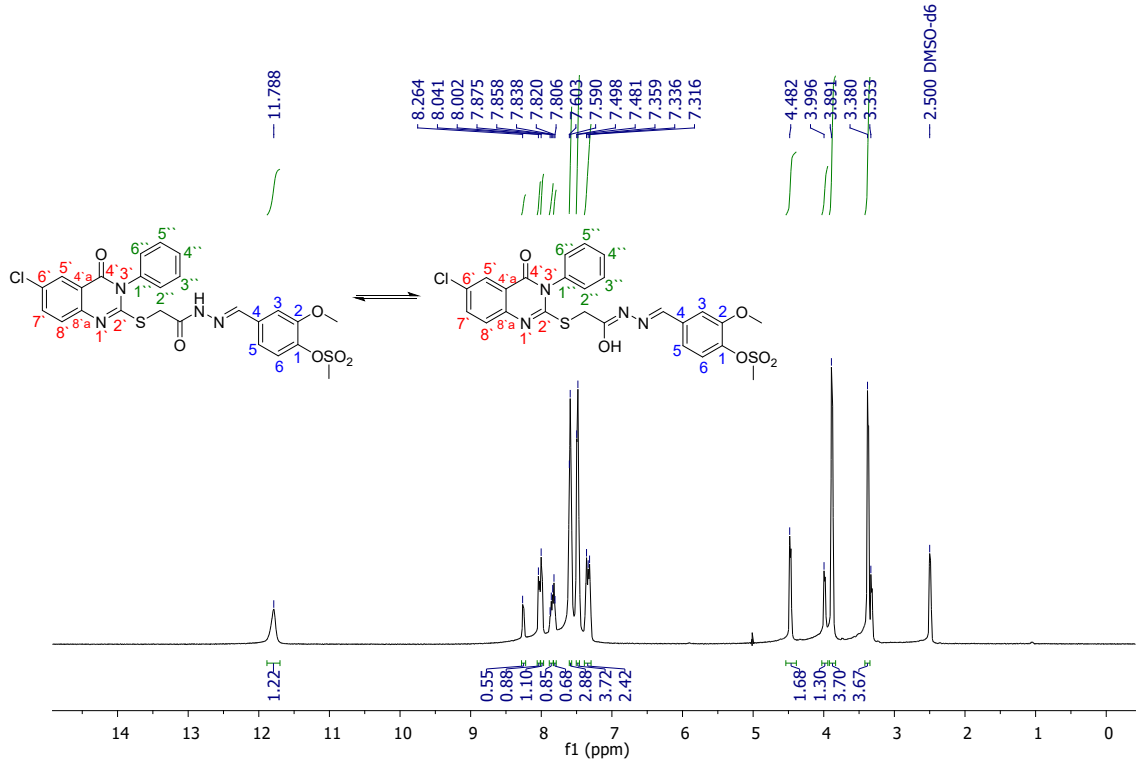

Fig. S26. ^{1}H NMR spectrum of compound **5m**.

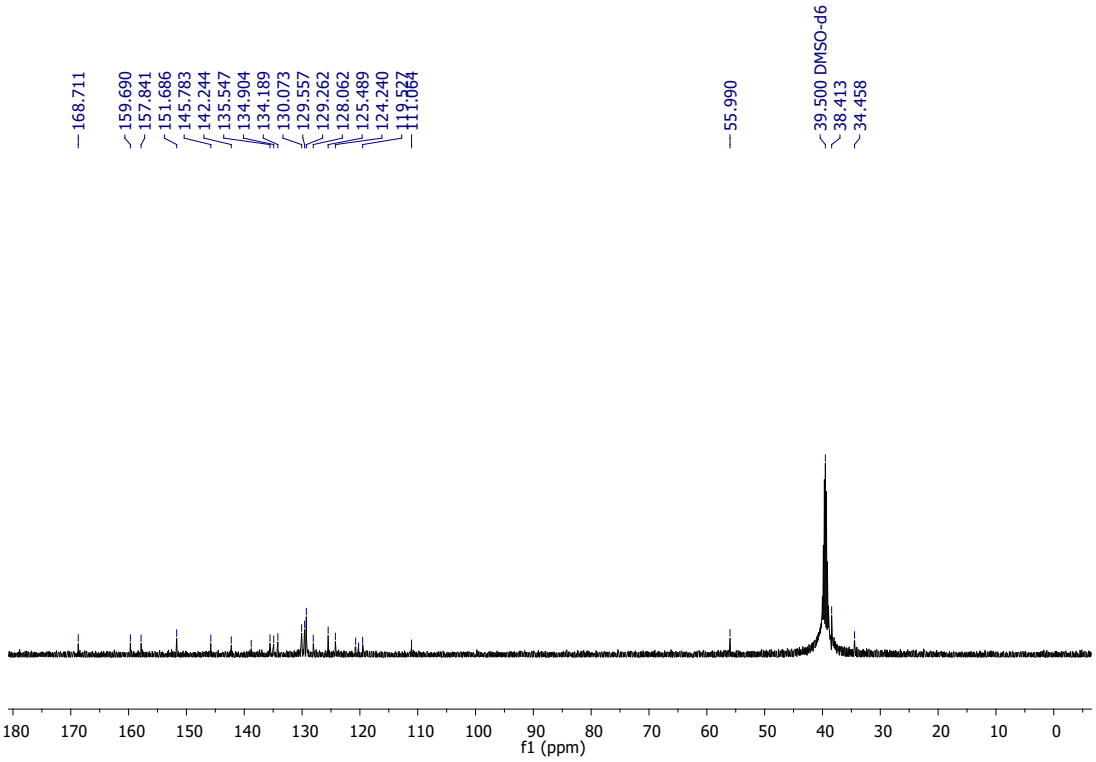

Fig. S27. ^{13}C NMR spectrum of compound **5m**.

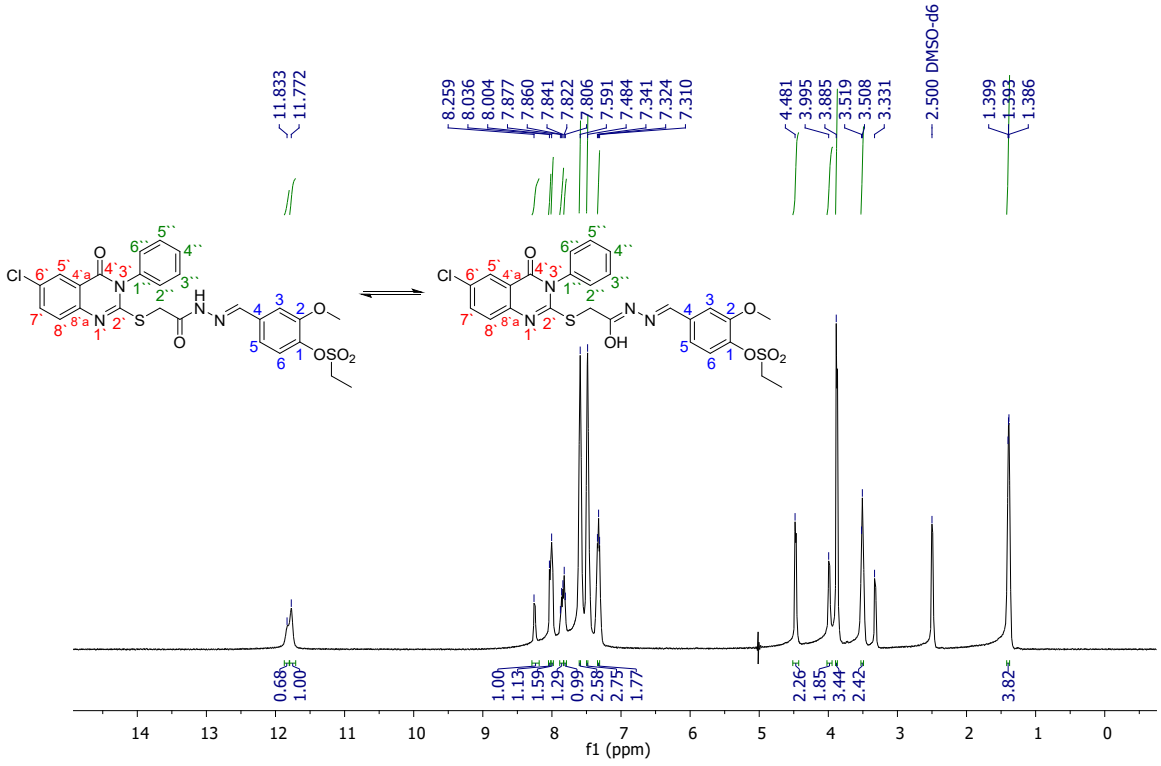

Fig. S28. ^{1}H NMR spectrum of compound **5n**.

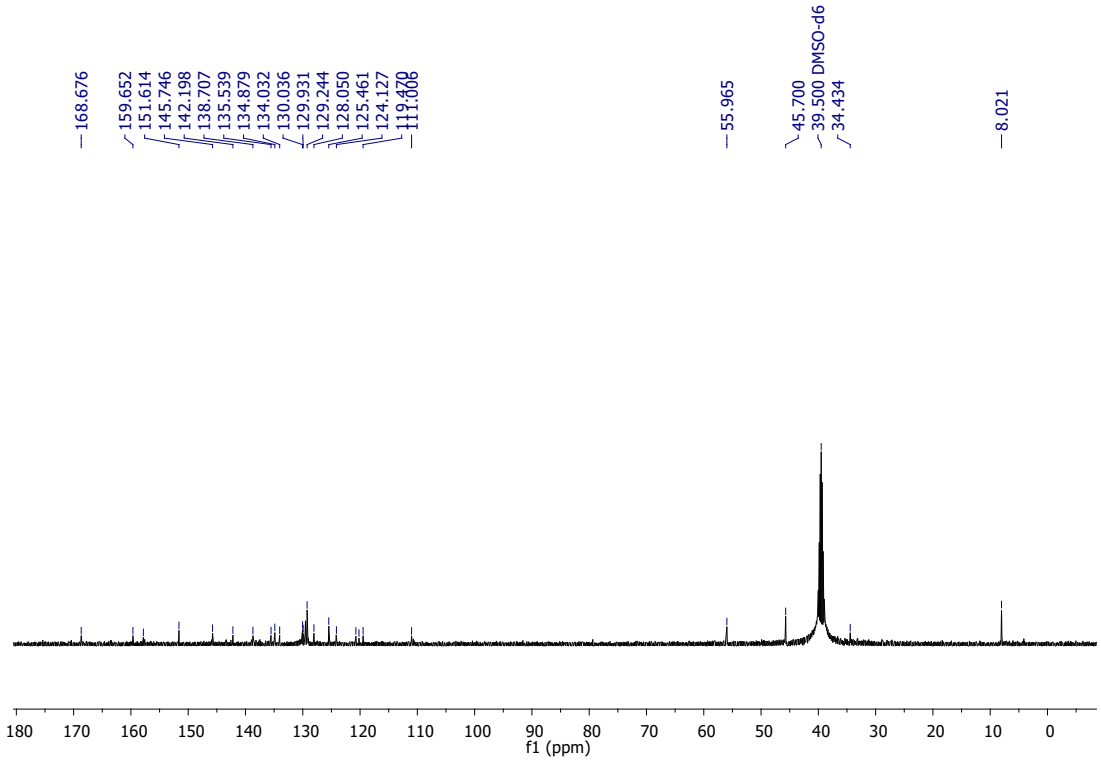

Fig. S29. ^{13}C NMR spectrum of compound **5n**.

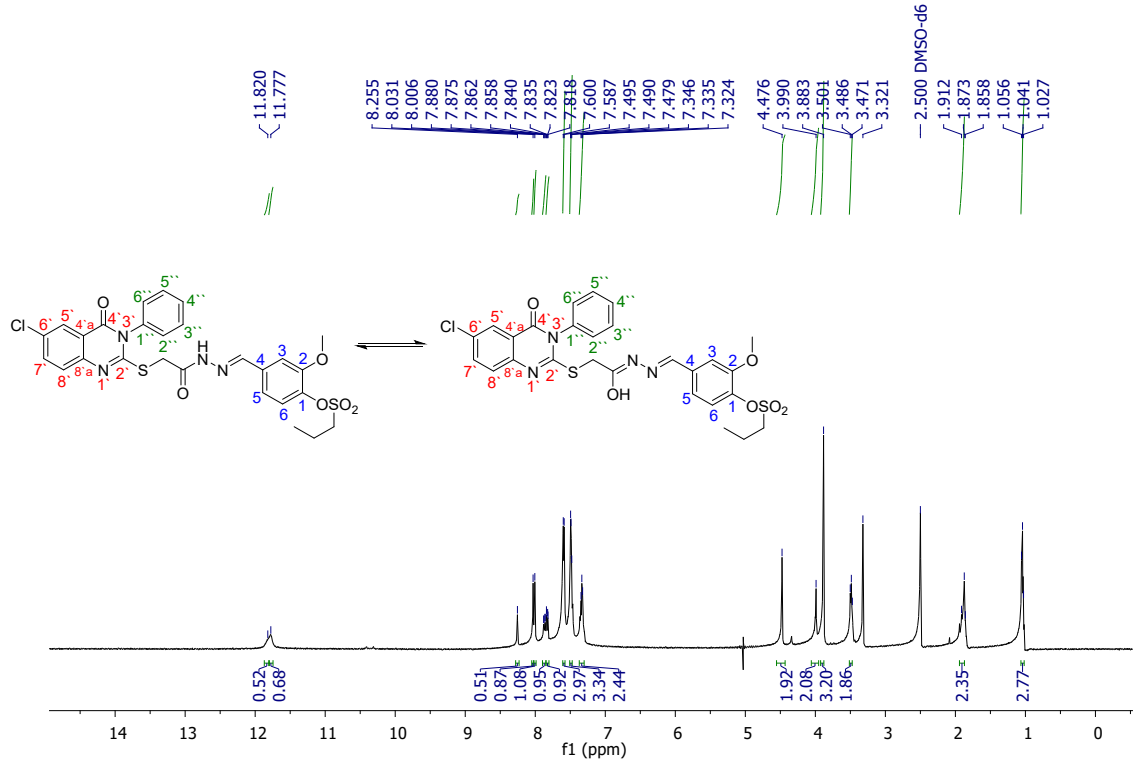

Fig. S30. ^{1}H NMR spectrum of compound **5o**.

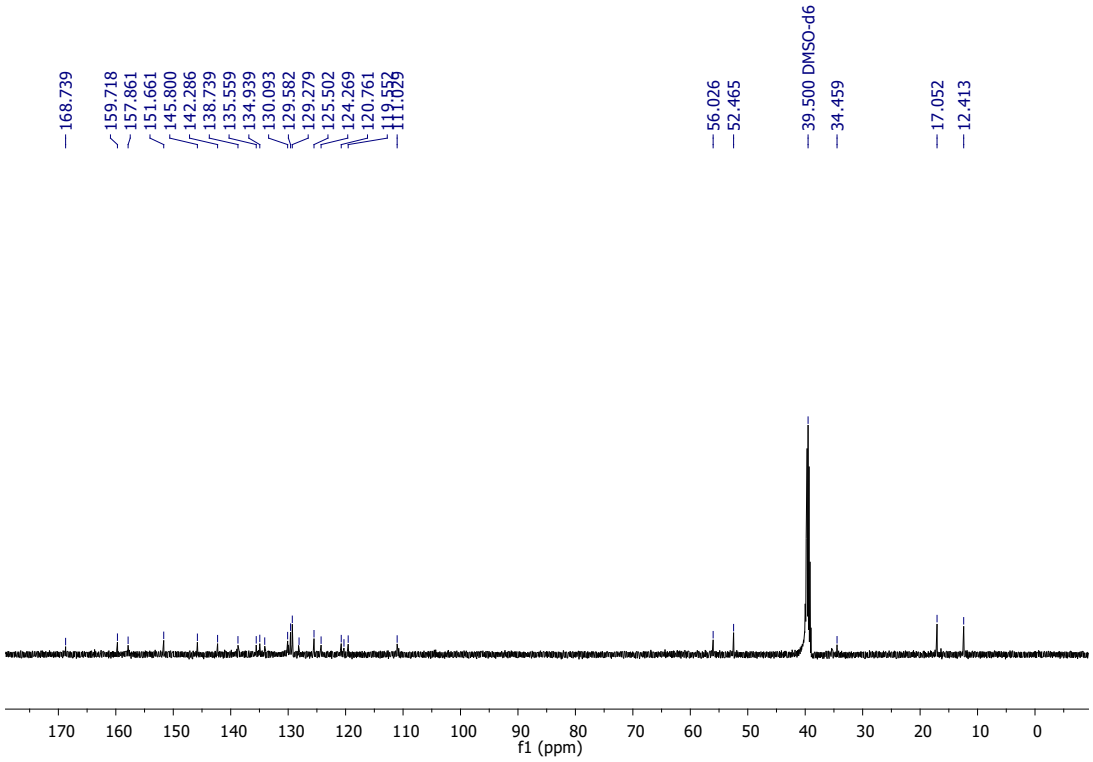

Fig. S31. ^{13}C NMR spectrum of compound **5o**.

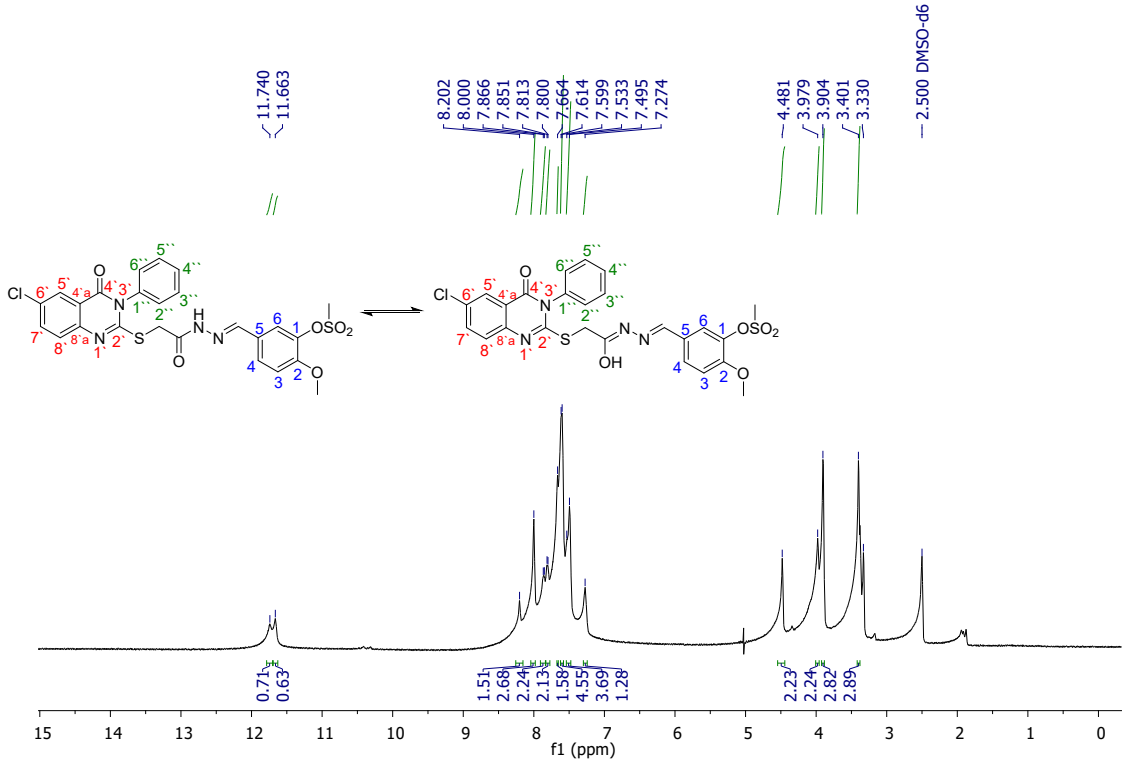

Fig. S32. ^{1}H NMR spectrum of compound **5p**.

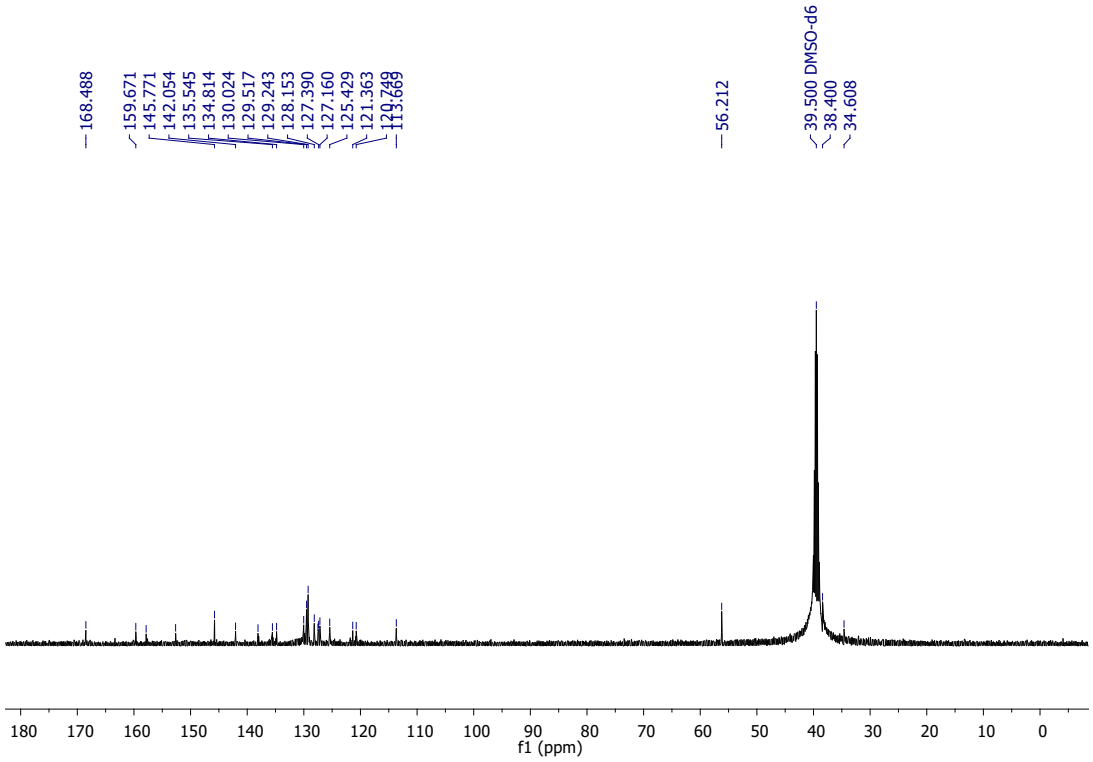

Fig. S33. ^{13}C NMR spectrum of compound **5p**.

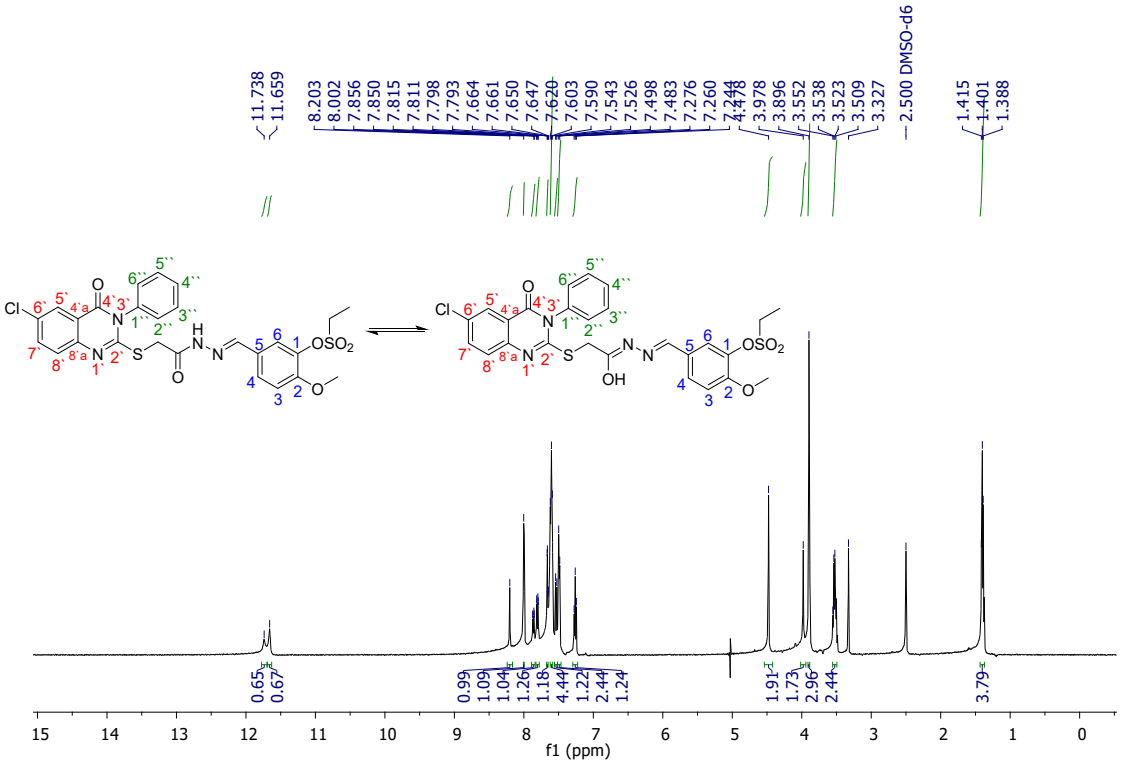

Fig. S34. ^{1}H NMR spectrum of compound **5q**.

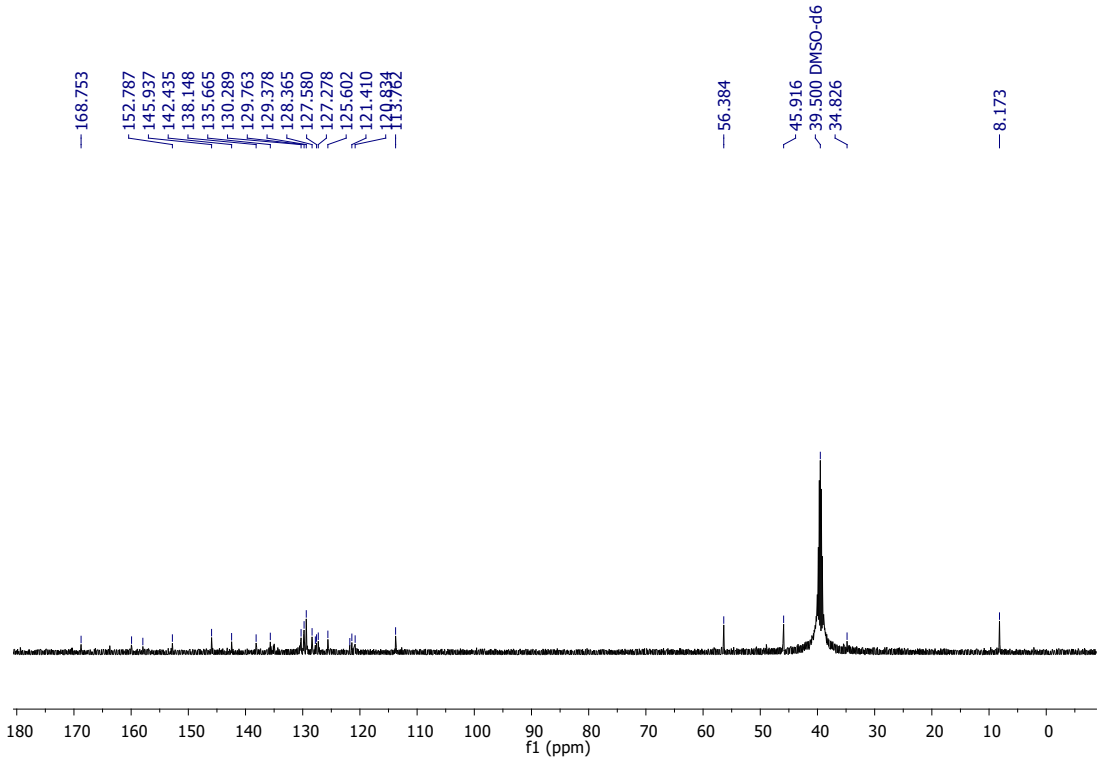

Fig. S35. ^{13}C NMR spectrum of compound **5q**.

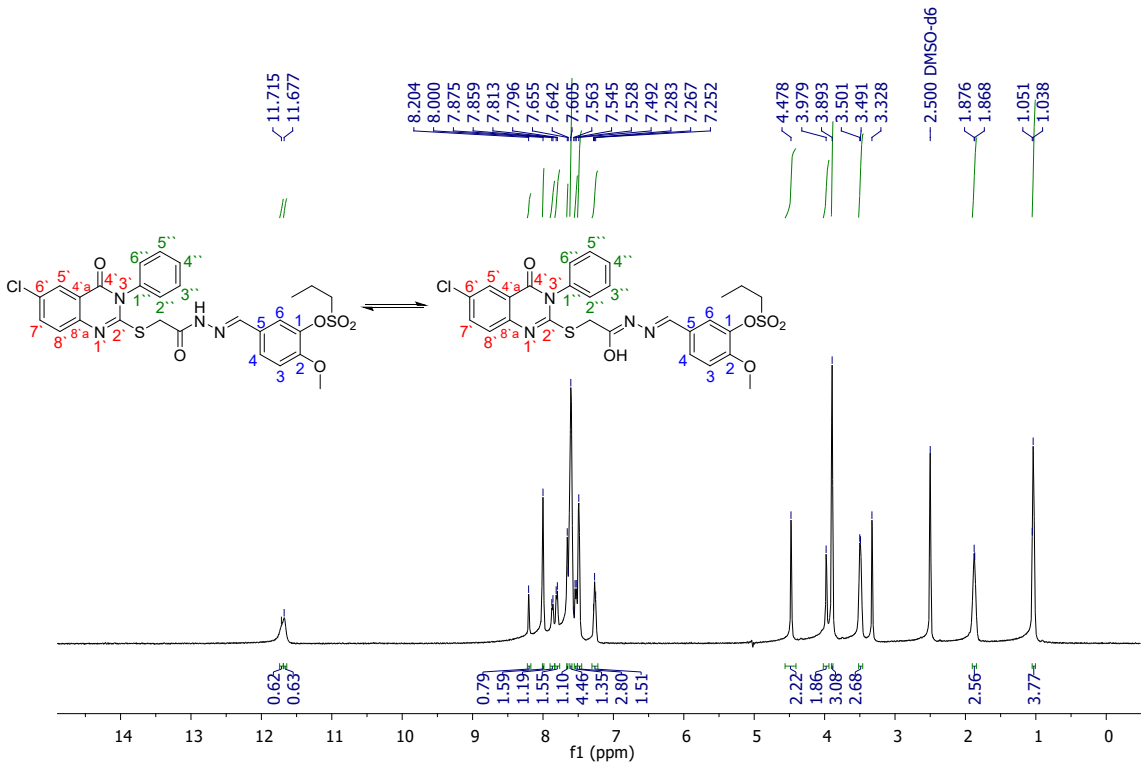

Fig. S36. ^{1}H NMR spectrum of compound **5r**.

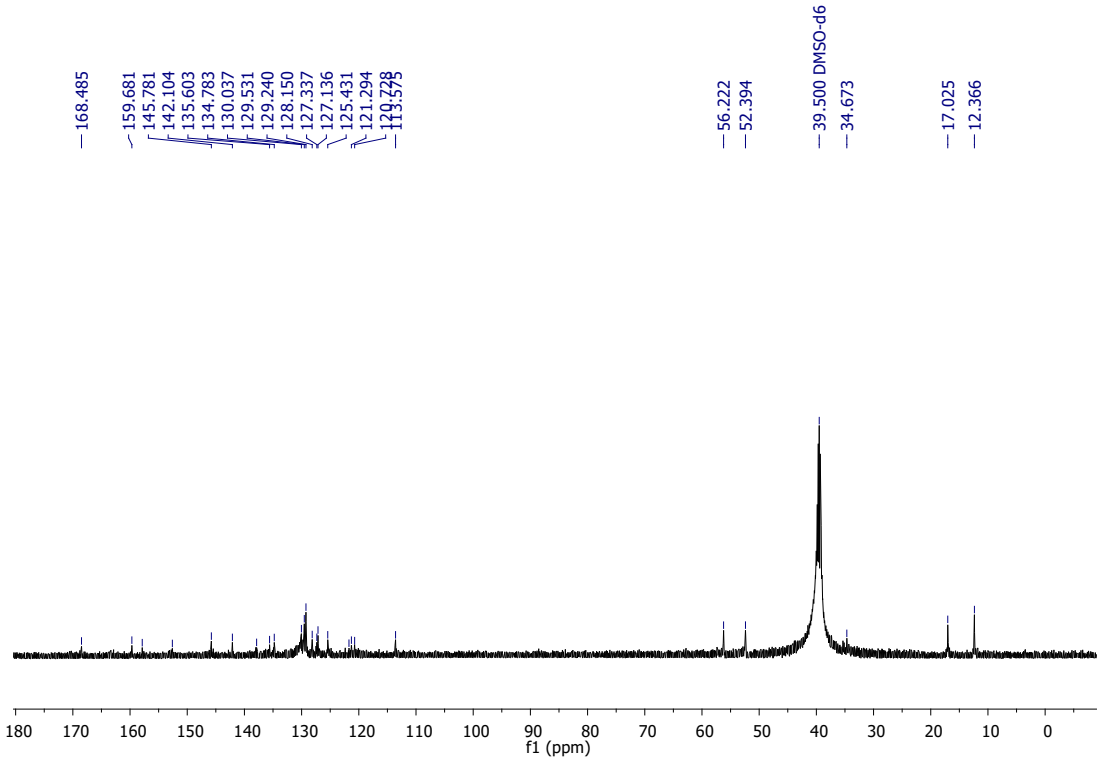

Fig. S37. ^{13}C NMR spectrum of compound **5r**.

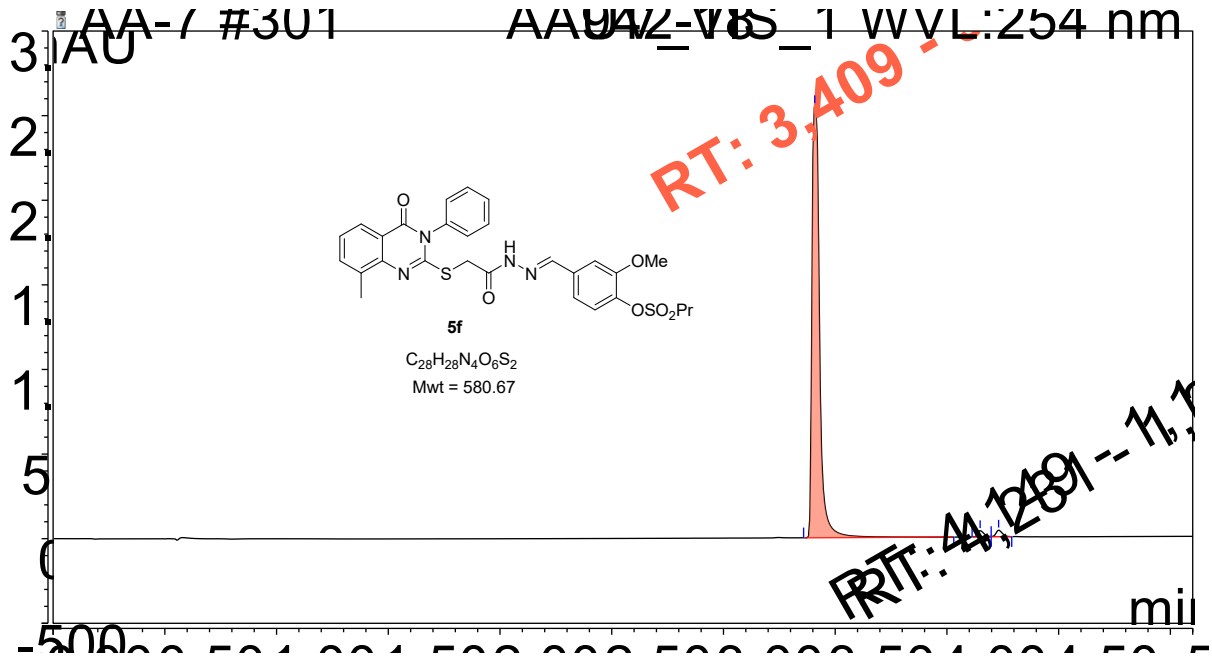

Fig. S38. HPLC purity of compound **5f**.

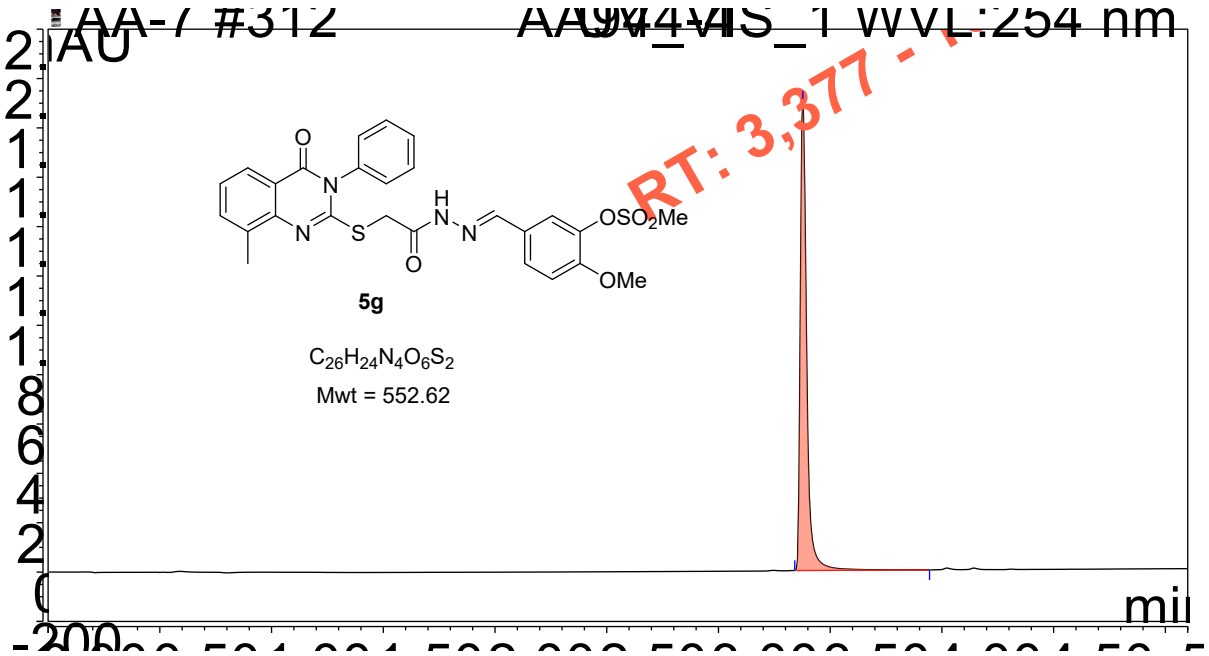

Fig. S39. HPLC purity of compound **5g**.

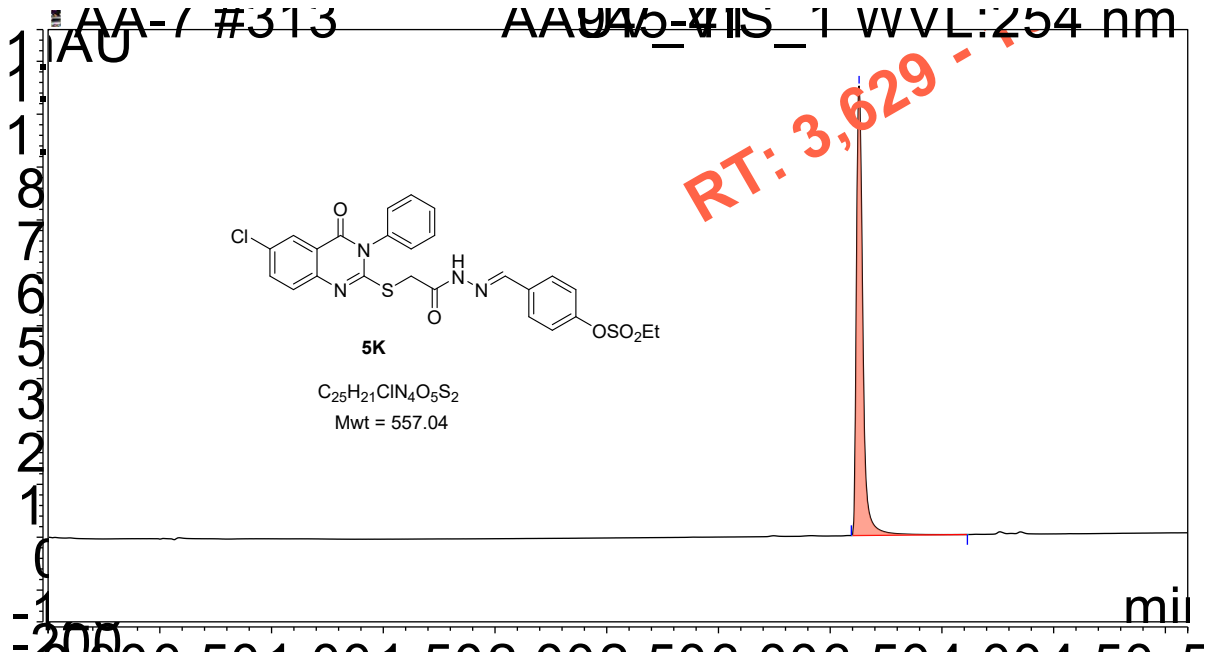

Fig. S40. HPLC purity of compound **5K**.

References

[1] S. S. Ragab, A. M. Sweed, Z. K. Hamza, E. Shaban, A. A. El-Sayed. Design, synthesis, and antibacterial activity of spiropyrimidinone derivatives incorporated

azo sulfonamide chromophore for polyester printing application, Fib. Polym. 23 (2022) 2114-2122. doi.org/10.1007/s12221-022-4032-4

[2] S. S. Ragab, M. Abdelraof, A. A. Elrashedy, A. M. Sweed. Design, synthesis, molecular dynamic simulation studies, and antibacterial evaluation of new spirocyclic aminopyrimidines, J. Mol. Struct. 1278 (2023) 134912. doi.org/10.1016/j.molstruc.2023.134912

[3] S. S. Ragab, N. E. Ibrahim, M. S. Abdel-Aziz, A. A. Elrashedy, A. K. Allayeh. Synthesis, biological activity, and molecular dynamic studies of new triazolopyrimidine derivatives. Results Chem. 6 (2023) 101163. doi.org/10.1016/j.rechem.2023.101163

[4] M. Mahran, N.A. Hassan, D.A.A. Osman, S.S. Ragab, A.A. Hassan. Synthesis and biological evaluation of novel pyrimidines derived from 6-aryl-5-cyano-2-thiouracil, Z. Naturforsch. C. J. Biosci. 71(5-6) (2016) 133-140. doi: 10.1515/znc-2015-0265

[5] S. Narramore, C. E. M. Stevenson, A. Maxwell, D. M. Lawson, C. W. G. Fishwick. New insights into the binding mode of pyridine-3-carboxamide inhibitors of E. coli DNA gyrase. Bioorg Med Chem. 2019 Aug 15;27(16):3546-3550. doi: 10.1016/j.bmc.2019.06.015

[6] A. Sabt, M. T. Abdelrahman, M. Abdelraof, H. R. M. Rashdan. Investigation of novel mucorales fungal inhibitors: synthesis, In-silico study and anti-fungal potency of novel class of coumarin-6-sulfonamides-thiazole and thiadiazole hybrids. Chemistry Select. 7 (17) (2022) e202200691. https://doi.org/10.1002/slct.202200691.

[7] S. X. T. Lianga, L. S. Wongb, Y. M. Limc, P. F. Leed, S. Djearamanea. Effects of Zinc Oxide nanoparticles on Streptococcus pyogenes. S. Afr. J. Chem. Eng. 34 (2020) 63-71. https://doi.org/10.1016/j.sajce.2020.05.009

[8] M. Abdelraof, M. S. Hasanin, M. M. Farag, H. Y. Ahmed. Green synthesis of bacterial cellulose/bioactive glass nanocomposites: Effect of glass nanoparticles on cellulose yield, biocompatibility and antimicrobial activity. Int. J. Biol. Macromol. 138 (2019) 975-985. doi: 10.1016/j.ijbiomac.2019.07.144.

[9] M. A. El-Bendary, M. Abdelraof, M. E. Moharam, E. M. Elmahdy, M. A. Allam, Potential of silver nanoparticles synthesized using low active mosquitocidal Lysinibacillus sphaericus as novel antimicrobial agents. Prep. Biochem. Biotech. 51 (9) (2021). 925-935. doi: 10.1080/10826068.2021.1875236.

[10] M. M. Qader, A. A. Hamed, S. Soldatou, M. Abdelraof, M. E. Elawady, A. S. I. Hassane, L. Belbahri, R. Ebel, M. E. Rateb. Antimicrobial and antibiofilm activities of the fungal metabolites isolated from the marine Endophytes Epicoccum nigrum M13 and Alternaria alternata 13A. Mar. Drugs. 19(4) (2021) 323. doi: 10.3390/md19040232.